mouse 3–4 days post-inoculation from frozen stock under drug pressure. Mice were infected with 25,000 parasitized red blood cells (pRBCs) intraperitoneally, unless otherwise indicated.

**Determination of parasitemia and hematocrit.** Blood samples were collected from experimental mice via the tail vein at the times indicated. Thin blood films were prepared and fixed with methanol followed by staining with Giemsa solution (Sigma, St. Louis, MO, USA). Parasitemia was determined by counting the percentage of pRBCs under a microscope, or by flow cytometry for mice infected with PyNL-GFP. Hematocrits were measured by centrifugation using a heparinized microhematocrit tube (Drummond microcaps; Drummond Scientific Company, Broomall, PA, USA).

**Antibodies.** PE-anti-TER119, APC-anti-TER119, PE-Cy7-anti-TER119, PE-anti-CD44, PE-anti-CD71, PE-anti-MHC class I and (PE)-anti-H-2K$^b$-SIINFEKL (25-D1.16) antibodies (eBioscience, San Diego, CA, USA) and FITC-anti GFP (abcam, Tokyo, Japan) were used for fluorescence microscopy or flow cytometry. Purified anti-CD16/32 (2.4G2) antibodies were also obtained from eBioscience. Anti-PE, anti-APC anti-CD11c and anti-CD8 microbeads (Miltenyi Biotech, Auburn, CA, USA) were used for magnetic cell-sorting (MACS) cell purification. Anti-IFN-γ capture and detection antibodies for enzyme-linked immunosorbent assays (ELISA) were obtained from R&D Systems (Minneapolis, MN, USA).

**Erythroblast induction and purification.** To stimulate erythroblast production *in vivo*, mice were injected intraperitoneally with 50 mg/kg weight of phenylhydrazine hydrochloride (PHZ, Kanto Chemical, Tokyo, Japan)[32,33]. To remove RBCs, the collected bone marrow or spleen cells were hemolyzed with ACK lysing buffer ($NH_4Cl$ 8024 mg/l, $KHCO_3$ 1001 mg/l, EDTA $Na_2{\cdot}2H_2O$ 3.722 mg/l), or with 0.2% NaCl, and adjusted to natural osmotic pressure with 1.6% NaCl. Hemolyzed samples were washed twice with medium then incubated with anti-CD16/32 (Fc-block) and stained with PE- or APC-anti-TER119 antibodies. Anti-PE or anti-APC microbeads were then added to the samples and the erythroblasts purified using MACS. Purified erythroblasts were used for flow cytometry, fluorescence microscopy, antigen presentation, and cytotoxicity assays. The sorted bone marrow or splenic erythroid precursor cell (TER119$^+$ cell) purity was > 90–95%. Parasitized erythroblasts were isolated from enriched erythroblasts from mice infected with PyNL-GFP-GFP or PyNL-GFP-OVA after further staining with PE-anti-MHC class I antibodies. GFP$^+$TER119$^+$ and GFP$^+$MHC class I$^{hi}$ cells were sorted using a FACSAria II cell sorter (Becton Dickinson, Mountain View, CA, USA) and used as non-parasitized and parasitized erythroblasts, respectively.

**Flow cytometry and fluorescence microscopy.** Peripheral blood, bone marrow and spleen cell suspensions, treated with or without lysing buffer, were incubated with Fc-block and stained with fluorochrome-labeled antibodies. Stained cells were analyzed using FACSCalibur flow cytometry (Becton Dickinson, Mountain View, CA, USA); data were analyzed using FlowJo software (Treestar, Ashland, OR, USA). Stained samples were fixed with 0.5% paraformaldehyde, smeared with cytospin 4 cytocentrifuge (Thermo Fisher Scientific, Waltham, MA, USA), then mounted with VECTASHIELD Mounting Medium and DAPI (Vector Laboratories, Burlingame, CA, USA). Samples were analyzed using a BIOREVO BZ-9000 microscope (KEYENCE, Osaka, Japan). Data were analyzed with BZ-II software (KEYENCE).

**Antigen presentation assays.** Splenic erythroblasts and TER119$^-$ splenocytes ($1 \times 10^7$ cells/ml) were pulsed with $10^{-6}$ M or the indicated dose of the OVA 8-mer CTL epitope (SIINFEKL) for 1 h at 37°C. Cells were washed three times with RPMI 1640 (Sigma). For MHC class I blocking experiment (Fig. 5e), cells were Fc-blocked and incubated with 1 μg/ml of anti-H-2K$^b$-SIINFEKL (25-D1.16) or control Abs for 30 min at 4°C, then washed with PRMI-1640. Cells were fixed by 0.5% para-formaldehyde and quenched by 0.1 M glycine, as standard method in antigen presentation assay[34]. Erythroblasts or TER119$^-$ splenocytes ($2 \times 10^4$ or the indicated number) were co-cultured with purified Rag2$^{-/-}$ OT-I CD8$^+$ CD11c$^-$ T cells ($10^5$) in a 200 μl final volume in a 96-well plate for 48–76 h or as indicated at 37°C in a $CO_2$ incubator with RPMI 1640 (Sigma) containing 10% fetal bovine serum, 2 mM L-glutamine, 1 mM sodium pyruvate, 0.1 mM non-essential amino acids, penicillin-streptomycin and 2-mercaptoethanol. Culture supernatants were collected to measure the IFN-γ released from CD8$^-$ T cells using ELISA.

**Cytotoxicity assays.** *In vitro* cytotoxicity assays were performed using VITAL[35]. Briefly, splenic erythroblasts or TER119$^-$ splenocytes were separated into two groups. One group ($1 \times 10^7$ cells/ml) was pulsed with $10^{-6}$ M OVA 8-mer peptide for 1 h at 37°C in a $CO_2$ incubator then stained with 250 nM 5-(and-6)-carboxyfluorescein diacetate, succinimidyl ester (CFSE, Molecular Probes, Invitrogen, Eugene, OR, USA) for 5 min at room temperature. The other group ($1 \times 10^7$ cells/ml) was stained with 2 μM PKH26 (Sigma) for 4 min at room temperature. Dead cells were removed from CFSE or PKH26 labeled cells using Lympholyte-M (Cedarlane Laboratories, Ontario, Canada). Living CFSE or PKH26 labeled cells were co-cultured for 4 h at 37°C in a $CO_2$ incubator with or without a variable number of primed CD8$^+$ T cells from OT-I mice that had been injected with 20 nmol of the OVA 8-mer peptide two days before the assay commenced. After co-culturing at the indicated ratio of OT-I cells, samples were stained with PI and analyzed using a flow cytometer. PI$^-$ cells were gated, and the mean percent survival of peptide pulsed target cells (CFSE$^+$) was calculated relative to non-pulsed target cells (PKH26$^+$). For MHC class I blocking experiment (Fig. 6e), cells were Fc blocked and co-cultured with 1 μg/ml of anti-H-2K$^b$-SIINFEKL (25-D1.16) or control Abs. All data were adjusted according to the following formula: % survival = 100 × CFSE$^+$ cell number/PKH26$^+$ cell number (5000 cells), % specific lysis = 100 − % survival.

**Statistical analysis.** Statistical evaluation of differences between the experimental groups was conducted using analysis of variance and two-tailed unpaired Student's t tests. $P < 0.05$ was considered statistically significant.


1. Snow, R. W., Guerra, C. A., Noor, A. M., Myint, H. Y. & Hay, S. I. The global distribution of clinical episodes of Plasmodium falciparum malaria. *Nature* **434**, 214–217 (2005).
2. Good, M. F., Xu, H., Wykes, M. & Engwerda, C. R. Development and regulation of cell-mediated immune responses to the blood stages of malaria: implications for vaccine research. *Annu Rev Immunol* **23**, 69–99 (2005).
3. Waitumbi, J. N., Opollo, M. O., Muga, R. O., Misore, A. O. & Stoute, J. A. Red cell surface changes and erythrophagocytosis in children with severe plasmodium falciparum anemia. *Blood* **95**, 1481–1486 (2000).
4. Abdalla, S. H. Peripheral blood and bone marrow leucocytes in Gambian children with malaria: numerical changes and evaluation of phagocytosis. *Ann Trop Paediatr* **8**, 250–258 (1988).
5. Haldar, K. & Mohandas, N. Malaria, erythrocytic infection, and anemia. *Hematology Am Soc Hematol Educ Program*, 87–93 (2009).
6. Chang, K. H. & Stevenson, M. M. Malarial anaemia: mechanisms and implications of insufficient erythropoiesis during blood-stage malaria. *Int J Parasitol* **34**, 1501–1516 (2004).
7. Chang, K. H., Tam, M. & Stevenson, M. M. Inappropriately low reticulocytosis in severe malarial anemia correlates with suppression in the development of late erythroid precursors. *Blood* **103**, 3727–3735 (2004).
8. Tamez, P. A., Liu, H., Fernandez-Pol, S., Haldar, K. & Wickrema, A. Stage-specific susceptibility of human erythroblasts to Plasmodium falciparum malaria infection. *Blood* **114**, 3652–3655 (2009).
9. Panichakul, T. *et al.* Production of erythropoietic cells in vitro for continuous culture of Plasmodium vivax. *Int J Parasitol* **37**, 1551–1557 (2007).
10. Ru, Y. X. *et al.* Invasion of erythroblasts by Pasmodium vivax: A new mechanism contributing to malarial anemia. *Ultrastruct Pathol* **33**, 236–242 (2009).
11. Chen, K. *et al.* Resolving the distinct stages in erythroid differentiation based on dynamic changes in membrane protein expression during erythropoiesis. *Proc Natl Acad Sci U S A* **106**, 17413–17418 (2009).
12. Otsuki, H. *et al.* Single amino acid substitution in Plasmodium yoelii erythrocyte ligand determines its localization and controls parasite virulence. *Proc Natl Acad Sci U S A* **106**, 7167–7172 (2009).
13. Weidanz, W. P., Melancon-Kaplan, J. & Cavacini, L. A. Cell-mediated immunity to the asexual blood stages of malarial parasites: animal models. *Immunol Lett* **25**, 87–95 (1990).
14. Podoba, J. E. & Stevenson, M. M. CD4$^+$ and CD8$^+$ T lymphocytes both contribute to acquired immunity to blood-stage Plasmodium chabaudi AS. *Infect Immun* **59**, 51–58 (1991).
15. Lundie, R. J. *et al.* Blood-stage Plasmodium infection induces CD8$^+$ T lymphocytes to parasite-expressed antigens, largely regulated by CD8alpha+ dendritic cells. *Proc Natl Acad Sci U S A* **105**, 14509–14514 (2008).
16. Lau, L. S. *et al.* Blood-Stage Plasmodium berghei Infection Generates a Potent, Specific CD8$^+$ T-Cell Response Despite Residence Largely in Cells Lacking MHC I Processing Machinery. *J Infect Dis* **204**, 1989–1996 (2011).
17. Howe, L. *et al.* Malaria parasites (Plasmodium spp.) infecting introduced, native and endemic New Zealand birds. *Parasitol Res* **110**, 913–923 (2012).
18. Stephens, R., Culleton, R. L. & Lamb, T. J. The contribution of Plasmodium chabaudi to our understanding of malaria. *Trends Parasitol* **28**, 73–82 (2012).
19. LaCrue, A. N., Scheel, M., Kennedy, K., Kumar, N. & Kyle, D. E. Effects of artesunate on parasite recrudescence and dormancy in the rodent malaria model Plasmodium vinckei. *PLoS One* **6**, e26689 (2011).
20. Dondorp, A. M. *et al.* Artemisinin resistance in Plasmodium falciparum malaria. *N Engl J Med* **361**, 455–467 (2009).
21. Groettrup, M. *et al.* A role for the proteasome regulator PA28alpha in antigen presentation. *Nature* **381**, 166–168 (1996).
22. Chen, C. Y., Pajak, L., Tamburlin, J., Bofinger, D. & Koury, S. T. The effect of proteasome inhibitors on mammalian erythroid terminal differentiation. *Exp Hematol* **30**, 634–639 (2002).
23. Imai, T. *et al.* Involvement of CD8$^+$ T cells in protective immunity against murine blood-stage infection with Plasmodium yoelii 17XL strain. *Eur J Immunol* **40**, 1053–1061 (2010).
24. Zhou, F. Molecular mechanisms of IFN-gamma to up-regulate MHC class I antigen processing and presentation. *Int Rev Immunol* **28**, 239–260 (2009).
25. Felli, N. *et al.* Multiple members of the TNF superfamily contribute to IFN-gamma-mediated inhibition of erythropoiesis. *J Immunol* **175**, 1464–1472 (2005).
26. Tamez, P. A., Liu, H., Wickrema, A. & Haldar, K. P. falciparum Modulates Erythroblast Cell Gene Expression in Signaling and Erythrocyte Production Pathways. *PLoS One* **6**, e19307 (2011).
27. Fisch, P., Handgretinger, R. & Schaefer, H. E. Pure red cell aplasia. *Br J Haematol* **111**, 1010–1022 (2000).

28. Takamura, S. *et al.* Premature terminal exhaustion of Friend virus-specific effector CD8$^+$ T cells by rapid induction of multiple inhibitory receptors. *J Immunol* **184**, 4696–4707 (2010).
29. Iwanaga, S. *et al.* Functional identification of the Plasmodium centromere and generation of a Plasmodium artificial chromosome. *Cell Host Microbe* **7**, 245–255 (2010).
30. Janse, C. J., Ramesar, J. & Waters, A. P. High-efficiency transfection and drug selection of genetically transformed blood stages of the rodent malaria parasite Plasmodium berghei. *Nat Protoc* **1**, 346–356 (2006).
31. Miyakoda, M. *et al.* Malaria-specific and nonspecific activation of CD8$^+$ T cells during blood stage of Plasmodium berghei infection. *J Immunol* **181**, 1420–1428 (2008).
32. Vannucchi, A. M. *et al.* Identification and characterization of a bipotent (erythroid and megakaryocytic) cell precursor from the spleen of phenylhydrazine-treated mice. *Blood* **95**, 2559–2568 (2000).
33. Socolovsky, M. *et al.* Ineffective erythropoiesis in Stat5a$^{-/-}$5b$^{-/-}$ mice due to decreased survival of early erythroblasts. *Blood* **98**, 3261–3273 (2001).
34. Imai, T. *et al.* Heat shock protein 90 (HSP90) contributes to cytosolic translocation of extracellular antigen for cross-presentation by dendritic cells. *Proc Natl Acad Sci U S A* **108**, 16363–16368 (2011).
35. Hermans, I. F. *et al.* The VITAL assay: a versatile fluorometric technique for assessing CTL- and NKT-mediated cytotoxicity against multiple targets in vitro and in vivo. *J Immunol Methods* **285**, 25–40 (2004).

## Acknowledgments

We thank Dr. Shiroh Iwanaga for his help in generating the PAC. This study was supported by grant-in-aid (24117504 to H.H., 24790399 to T.I.) and the Strategic Fund for the Promotion of Science and Technology to H.H. from the Ministry of Education, Culture, Sports, Science and Technology of Japan and the Ministry of Health, Labour and Welfare of Japan (H24-Shitei-004) to H.H., and a Research Grant for Basic Medical Sciences from the Gunma Medical Association to T.I, and the Takeda Memorial Foundation to H.H., and Gunma University Operational Grants for multi-drug resistance to H.H.

## Author contributions

Contribution: T.I. performed the experiments, analyzed the results, created the figures, and wrote the manuscript; H.I. and M.H. generated the recombinant parasites; K.S. analyzed the results; T.T., H.O., T.S. and C.S. performed the experiments; and H.H. directed the project, analyzed the results and wrote the manuscript.

## Additional information

**Supplementary information** accompanies this paper at http://www.nature.com/scientificreports

**Competing financial interests:** The authors declare no competing financial interests.



**How to cite this article:** Imai, T. *et al.* CD8$^+$ T cell activation by murine erythroblasts infected with malaria parasites. *Sci. Rep.* **3**, 1572; DOI:10.1038/srep01572 (2013).

# Resistance to Malaria by Enhanced Phagocytosis of Erythrocytes in LMP7-deficient Mice

**Xuefeng Duan[1], Takashi Imai[2], Bin Chou[1], Liping Tu[1], Kunisuke Himeno[1], Kazutomo Suzue[2], Makoto Hirai[2], Tomoyo Taniguchi[2], Hiroko Okada[2], Chikako Shimokawa[2], Hajime Hisaeda[2]***

1 Department of Parasitology, Graduate School of Medical Sciences, Kyushu University, Fukuoka, Japan, 2 Department of Parasitology, Graduate School of Medicine, Gunma University, Maebashi, Japan

## Abstract

General cellular functions of proteasomes occur through protein degradation, whereas the specific function of immunoproteasomes is the optimization of antigen processing associated with MHC class I. We and others previously reported that deficiency in subunits of immunoproteasomes impaired the activation of antigen-specific $CD8^+$ T cells, resulting in higher susceptibility to tumor and infections. We demonstrated that $CD8^+$ T cells contributed to protection against malaria parasites. In this study, we evaluated the role of immunoproteasomes in the course of infection with rodent malaria parasites. Unexpectedly, *Plasmodium yoelii* infection of mice deficient in LMP7, a catalytic subunit of immunoproteasomes, showed lower parasite growth in the early phase of infection and lower lethality compared with control mice. The protective characteristics of LMP7-deficient mice were not associated with enhanced immune responses, as the mutant mice showed comparable or diminished activation of innate and acquired immunity. The remarkable difference was observed in erythrocytes instead of immune responses. Parasitized red blood cells (pRBCs) purified from LMP7-deficient mice were more susceptible to phagocytosis by macrophages compared with those from wild-type mice. The susceptibility of pRBC to phagocytosis appeared to correlate with deformity of the membrane structures that were only observed after infection. Our results suggest that RBCs of LMP7-deficient mice were more likely to deform in response to infection with malaria parasites, presumably resulting in higher susceptibility to phagocytosis and in the partial resistance to malaria.

**Citation:** Duan X, Imai T, Chou B, Tu L, Himeno K, et al. (2013) Resistance to Malaria by Enhanced Phagocytosis of Erythrocytes in LMP7-deficient Mice. PLoS ONE 8(3): e59633. doi:10.1371/journal.pone.0059633

**Editor:** Cevayir Coban, Osaka University, Japan

**Received** January 21, 2013; **Accepted** February 15, 2013; **Published** March 19, 2013



**Funding:** This work was supported by grants-in-aid (24117504), the Strategic Fund for the Promotion of Science and Technology, and Gunma University Operation Grants for the multi-drug resistance from the Ministry of Education, Culture, Sports, Science and Technology of Japan, and the Takeda Memorial Foundation. The funders had no role in study design, data collection and analysis, decision to publish, or presentation of the manuscript.

**Competing Interests:** The authors have declared that no competing interests exist.

* E-mail: hisa@gunma-u.ac.jp

## Introduction

The proteasome, a multicatalytic protease complex, is an essential component of the ATP-dependent proteolytic pathway that catalyzes the elimination of ubiquitinated proteins [1]. It is distributed in the nucleus and cytosol, where it can comprise 0.5 to 1.0% of total cellular protein [2]. The mammalian 26S proteasome is composed of a 20S proteolytic core consisting of two outer α rings, two inner β rings, and two additional 19S regulatory complexes. The 26S proteasome catalyzes the rapid degradation of proteins that are covalently linked to polyubiquitin chains. This pathway is highly regulated and selective, and in turn it regulates many important cellular processes such as transcriptional activation [3], cell-cycle progression [4], cell proliferation [5–7], differentiation [8,9] and apoptosis [10,11]. From the immunological point of view, proteasomal degradation of proteins is indispensable for antigen presentation associated with MHC class I, which activates $CD8^+$ T cells [12].

Interferon (IFN)-γ is an immunomodulatory cytokine produced by activated $CD4^+$ T cells, natural killer (NK) cells, and $CD8^+$ T cells that enhances antigen presentation by activating proteasome subunits and regulators in addition to up-regulating the expression of MHC and TAP genes. IFN-γ alters proteasome activity by incorporation of three IFN-γ-inducible catalytic subunits, LMP2, LMP7, and MECL-1 to replace the constitutive catalytic subunits (Y/δ, X/MB1, and Z, respectively) in the 20S core particle during proteasome biogenesis [13–20]. These IFN-γ-induced immunoproteasomes are thought to be more favorable for antigen presentation than constitutive proteasomes because the subunits induced by IFN-γ contain chymotrypsin activity that cleaves hydrophobic, basic and branched chain residues instead of acidic residues [16,21–23]. The importance of immunoproteasomes in MHC class I-associated antigen presentation has been proven using mice deficient for the IFN-γ-inducible subunits. Mice deficient in LMP7, a molecule responsible for major chymotrypsin activity, exhibited attenuated antigen presenting activity [24]. We previously showed that LMP7 plays a crucial role in inducing antigen-specific $CD8^+$ T cells, and LMP7-deficient mice were more susceptible to tumors [25] and protozoan infection [26,27], where CD8 T cells mainly function as effector cells.

Malaria remains a crucial threat to public health worldwide. It is well accepted that antibodies and $CD4^+$ T cells play critical roles in protection against blood-stage malaria that can be acquired during natural or experimental infection [28–31]. In addition, innate immunity attributed to macrophages, NK cells and

dendritic cells (DCs) is also important. Especially, phagocytosis exerted by macrophages residing in the reticuloendothelial system is crucial for the elimination of parasitized red blood cells (pRBCs). In contrast, the contribution of $CD8^+$ T cells to protective immunity against blood-stage malaria is controversial. Although RBCs are exceptional cells that express no MHC class I molecules, $CD8^+$ T cells are activated during blood-stage malaria [32,33]. Furthermore, activation of $CD8^+$ T cells is required for the development of experimental cerebral malaria [34]. We recently found that CD8 T cells are important for immunity against blood-stage malaria [35], leading us to hypothesize that LMP7-deficiency impairs resistance to infection with blood-stage malaria.

In this study, we observed that LMP7-deficient mice were partially resistant to infection with rodent malaria parasites, *Plasmodium yoelii*. We examined immune responses in LMP7-deficient mice in detail and found no explainable difference in innate and adaptive immunity including CD8 T cell responses. However, we found that pRBCs from LMP7-deficient mice were highly phagocytosed.

## Materials and Methods

### Ethics Statement

All experiments that involved mice were reviewed and approved by the Committee for Ethics on Animal Experiments in the Graduate School of Gunma University (approved number 12-031), and were conducted under the control of the Guidelines for Animal Experiments in the Graduate School of Medicine, Gunma University, and the Law (No. 105) and Notification (No. 6) of the Japanese Government.

### Mice and Parasites

C57BL/6 mice were purchased from Kyudo (Tosu, Japan). Immunoproteasome subunit LMP7-deficient (LMP7-deficient) mice on a C57BL/6 background were established [24] and provided by Dr. Fehling HJ (Ulm University, Germany). Age- and sex-matched groups of wild-type (WT) and LMP7-deficient mice were used for the experiments. Blood-stage parasites of *Plasmodium yoelii* 17XL(PyL) or 17XNL (PyNL) were obtained after fresh passage through a donor mouse 2–3 days after inoculation with a frozen stock. Mice were infected intraperitoneally with 25,000 parasitized pRBCs.

pRBCs were separated using a Percoll gradient after removal of leukocytes, as previously described [36]. Briefly, heparinized blood from malaria-infected mice was collected after heart puncture, and passed through a CF11 column to remove white blood cells. The eluent RBC solution was placed onto 58% (v/v) Percoll/PBS and centrifuged, and cells at the interphase or at the bottom were collected as schizont-rich pRBCs or schizont-free RBCs, respectively.

### Fluorescence-activated Cell Sorting (FACS) Analysis

The following antibodies (Abs) were obtained from eBioscience (San Diego, CA) and used to assess cell surface or intracellular expression of their respective antigens: allophycocyanin (APC)-conjugated anti-mouse CD3ε (145-2C11), APC-, FITC-, and PE-conjugated anti-mouse CD4 (GK1.5), PE-conjugated anti-mouse CD11b (M1/70), FITC-conjugated anti-mouse CD11c (N418), PE-Cy5-conjugated anti-mouse CD40 (1C10), FITC-conjugated anti-mouse CD69 (H1.2F3), APC-conjugated anti-mouse CD80 (16-10A1), APC-conjugated anti-mouse CD86 (GL1), PE-Cy5-conjugated anti-mouse $I\text{-}A^b$ MHC class II (M5/144.15.2), and PE-conjugated anti-mouse IFN-γ (XMG1.2). Stained cells were analyzed using FACSCalibur flow cytometer (BD Bioscience, San Jose, CA), and the list data were analyzed using CellQuest Pro software (BD Biosciences).

### Quantitative real-time PCR

mRNA quantification of IFN-γ was performed with a real-time PCR system (Applied Biosystems, Foster City, CA), using SYBR Green I double-strand DNA binding dye. Total RNA extracted from $1\times10^7$ splenocytes from an uninfected or infected mouse (5 days after infection) was reverse-transcribed followed by PCR. For IFN-γ, the sense and antisense primers were 5′-AGCGGCT-GACTGAACTCAGATTGTAG-3′ and 5′-GTCACAGTTTT-CAGCTGTATAGGG, respectively. Fluorescence data collected after each extension step were analyzed using an ABI Prism 7000 SDS software. The relative ratio of mRNA encoding IFN-γ in each sample was normalized to the relative quantity of β-actin.

### Phagocytosis of Macrophages

Peritoneal macrophages were collected from WT and LMP7-deficient mice 4 days after injection with 0.5 ml thioglycollate solution. RBCs ($10^7$ cell/ml) were incubated with 10 μM carboxyfluorescein succinimidyl ester (CFSE) in PBS for 15 min at 37°C. CFSE staining was stopped by addition excess complete medium (fetal bovine serum-supplemented RPMI1640) and washing cells three times with complete medium. Macrophages ($5\times10^5$ or $4\times10^5$ cells/well) were cultured with $5\times10^6$ CFSE-labeled RBCs at a final volume of 200 μl for 1 h at 37°C. After co-culture, non-ingested RBCs were removed by hemolysis with $NH_4Cl$ lysing buffer. The remaining macrophages were washed twice with complete medium, and then stained with PE-conjugated anti-mouse CD11b Ab before flow cytometric analysis.

### Scanning Electron Microscopy (SEM)

The surface of RBCs was examined by SEM. RBCs from WT or LMP7-deficient mice were washed with PBS by repeated centrifugation at 1,000 × *g* for 10 min to remove contaminating cell debris and were then fixed with 1.5% glutaraldehyde. The specimen was then dehydrated in a series of acetone solutions and finally with amyl acetate. After critical point drying (JCPD2, JEOL), the RBC specimen was coated with gold-palladium for surface conductivity and examined by the scanning mode of the electron microscope (EMASID20 combined with JEM2000EX, JEOL) at 25 kV.

### Statistics

Differences between groups were analyzed for statistical significance with unpaired Student *t*-tests. For survival curves, Kaplan-Meier plots were performed. All of these were performed using Excel software. Probabilities below 0.05 were considered statistically significant.

## Results

### LMP7-deficient Mice are Partially Resistant to Infection with Malaria Parasites

We first infected LMP7-deficient mice with rodent malaria parasites, *P. yoelii* 17XL (PyL) and *P. yoelii* 17XNL (PyNL). As previously reported, rapid growth of PyL parasites occurred in WT mice, and all mice infected with PyL succumbed to the infection within 2 weeks (Fig. 1A). Surprisingly, LMP7-deficient mice were partially resistant to the normally lethal infection. More than half of the LMP7-deficient mice tolerated the peak of parasitemia and survived (Fig. 1A). The resistance of LMP7-deficient mice was also observed when infected with PyNL.

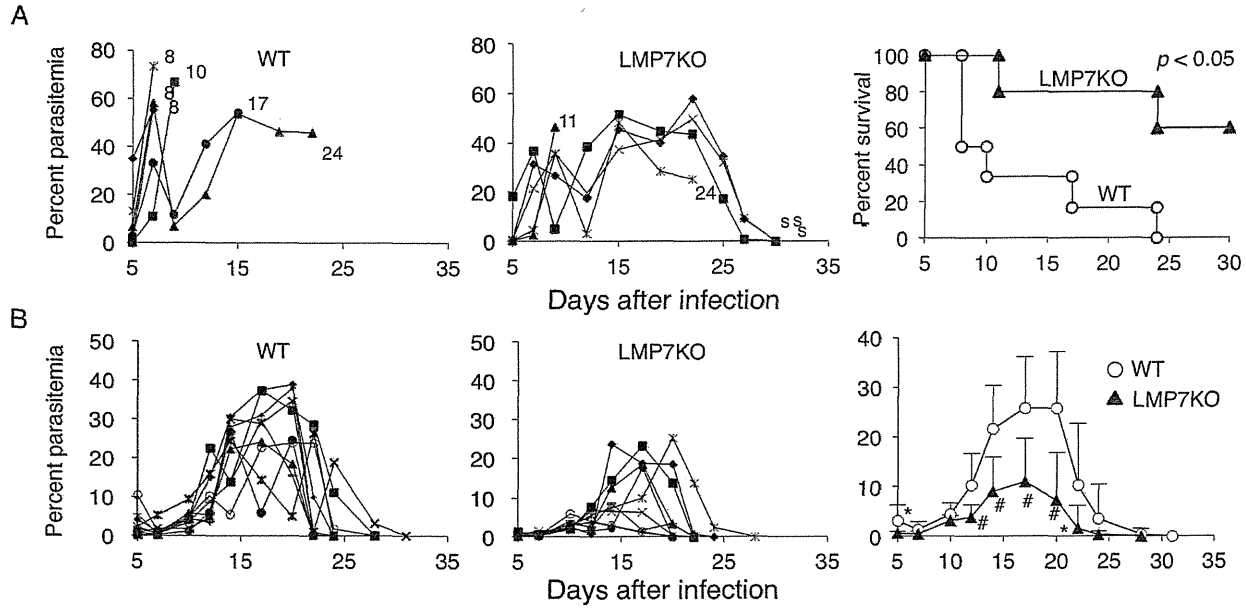


**Figure 1. Resistance of LMP7-deficient mice to infection with *P. yoelii*.** (**A**) Parasitemia (two left panels) and survival ratio (right panel) was monitored in the indicated mice infected with PyL. Each symbol represents parasitemia from an individual mouse, and the numbers or "s" represent day of mouse death or mice survival, respectively. (**B**) Infection with PyNL was analyzed as in A. The right panel shows mean parasitemia+SD of seven WT (open circles) and LMP7-deficient (triangles) mice. *,# $p<0.05$ or $p<0.01$ indicate significant difference between WT and LMP7-deficient mice using the Student's *t*-test, respectively. Similar results were obtained from three repeated experiments.
doi:10.1371/journal.pone.0059633.g001

Infection with PyNL caused a transient infection with a peak parasitemia up to 30% followed by complete eradication in WT mice (Fig. 1B). LMP7-deficient mice infected with PyNL showed a significantly lower level of parasitemia during the course of infection and took a shorter time to recover from the infection (Fig. 1B).

## Resistance of LMP7-deficient Mice is not Due to Enhancement of Adaptive Immunity

LMP7-deficient mice were unexpectedly more resistant to malaria disease. To determine the mechanisms underlying resistance in LMP7-deficient mice, we analyzed immune responses in mice infected with PyL. We previously showed that LMP7-deficient mice have no defect in the number or proportions of $CD4^+$ and $CD8^+$ T cells in lymphoid organs compared with WT mice (26). As T cell-mediated immune responses are indispensable for protection against malaria, we first examined the activation of T cells by determining expression of CD69, an early activation marker. Splenic $CD4^+$ and $CD8^+$ T cells expressing CD69 were increased in response to infection with PyL in WT mice. Similarly, infection of LMP7-deficient mice activated T cells comparable to WT mice (Fig. 2A). We next analyzed the functional properties of T cells. Since IFN-γ produced by T cells is important for protection against blood-stage malaria, we examined IFN-γ production during malaria. Real-time RT-PCR analyses revealed that mRNA levels encoding IFN-γ in spleens of LMP7-deficient mice were indistinguishable from those of WT mice before and after infection with PyL (Fig. 2B). We next performed intracellular FACS analyses to confirm production of IFN-γ protein. Infection with PyL clearly increased the number of $CD3^+CD4^+$ and $CD3^+CD4^-$ (almost $CD8^+$) cells that expressed IFN-γ (Fig. 2C). Although similar numbers of $CD4^+$ T cells producing IFN-γ were found in LMP7-deficient mice compared to WT mice they contained less IFN-γ producing $CD8^+$ T cells than WT mice (Fig. 2D). This might be caused by the less-efficient generation of antigenic epitopes for $CD8^+$ T cells due to the lack of LMP7, resulting in the failure of full activation of functional $CD8^+$ T cells. However, we did not observed enhanced adaptive immune responses that could explain the increased resistance to malaria observed in LMP7-deficient mice.

## Resistance of LMP7-deficient Mice is not Due to Enhancement of Innate Immunity

Since LMP7-deficient mice showed a significant lower parasitemia in the early phase of infection, which was not due to differences in adaptive immunity, we next analyzed innate immune responses exerted by DCs and macrophages. Activation of DCs critical for driving adaptive immunity occurred in both WT and LMP7-deficient mice at 5 days after infection with PyL. The degree of activation was lower in LMP7-deficient mice in terms of expression of DC activation markers (Fig. 3A). These results suggested that DCs were less activated in response to lower levels of parasites, because the level of parasitemia was significantly low at this time point in LMP7-deficient mice. Thus, activation of DCs could not explain the enhanced protection in LMP7-deficient mice.

Therefore, we tried to examine more primitive host defense mechanism against malaria parasites, the phagocytosis of pRBCs by macrophages. Macrophages are thought to be crucial effectors for eliminating pRBCs or free merozoites, by phagocytosis followed by their digestion in phagosomes. Schizont-rich pRBCs purified from WT mice using Percoll gradient were labeled with CFSE, cultured with macrophages, and their phagocytic ability assessed by CFSE incorporation. Phagocytosis of pRBCs by LMP-deficient macrophages was comparable to WT macrophages (Fig. 3B). Macrophages phagocytosed low numbers of RBCs from

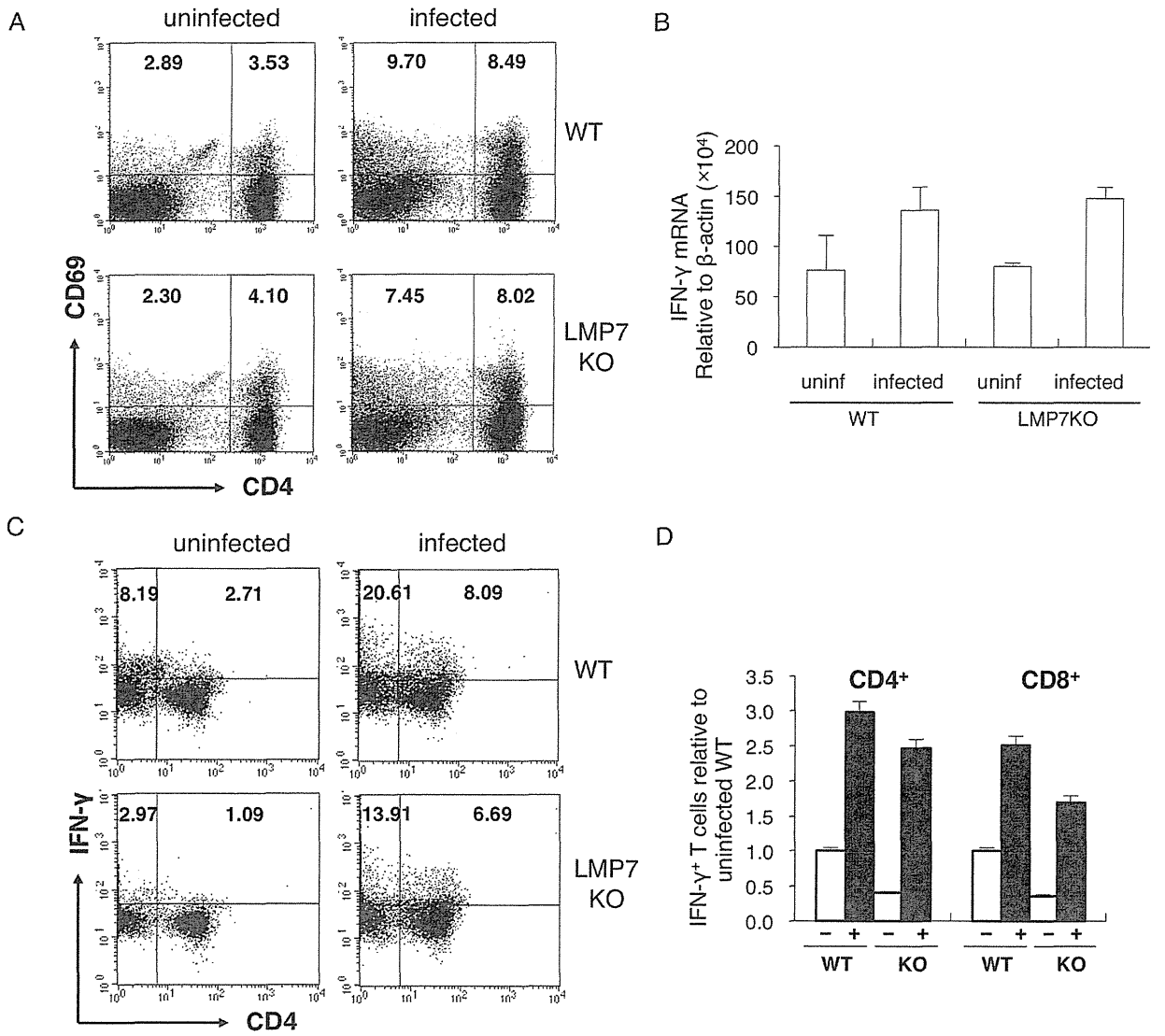


**Figure 2. Comparable adaptive immune responses to malaria parasites in LMP7-deficient mice.** Spleen cells isolated from WT and LMP7-deficient mice 5 days after infection were analyzed. (**A**) Splenocytes stained with fluorochrome-conjugated anti-CD3, anti-CD4, and anti-CD69 were analyzed for activation of T cells. Gated $CD3^+$ cells were separated by CD4 and CD69 expression. The $CD4^-$ cell population contained mostly $CD8^+$ cells. Numbers represent the percentage of all cells in each quadrant. (**B**) mRNA encoding IFN-γ in total RNA extracted from splenocytes of the indicated mice was quantified by real-time PCR. Values represent the relative quantities of mRNA encoding genes of interest to that of β-actin and mean ± SD of 3 mice. (**C**) Production of IFN-γ in splenic T cells of the indicated mice was analyzed. Gated $CD3^+$ cells were separated by CD4 and IFN-γ expression. Numbers represent the percentage of all cells in each quadrant. (**D**) Absolute numbers of IFN-γ-producing cells were also calculated (bar graph). Values indicate mean ± SD of 3 mice. Results are representative of at least two independent experiments.
doi:10.1371/journal.pone.0059633.g002

uninfected mice (Fig. 4A), suggesting that they specifically recognize some alterations in RBCs associated with infection by malaria parasites.

## RBCs of LMP7-deficient Mice are More Susceptible to Phagocytosis by Macrophages

Surprisingly, phagocytosis was remarkably enhanced when pRBCs from LMP7-deficient mice were used compared with those from WT mice (Fig. 4A), indicating that LMP7-deficient RBCs could be phagocytosed more easily by macrophages. This enhancement of phagocytosis was observed only when mice were infected with malaria parasites, as RBCs from uninfected LMP7-deficient mice were phagocytosed comparably to that from uninfected WT mice (Fig. 4A). These results suggested a difference in structure between WT and LMP7-deficient RBCs after infection. To explore the reasons why LMP7-deficient pRBCs were more sensitive to phagocytosis, we evaluated the morphology of RBCs infected with PyL using SEM. Before infection, there was no visible difference in RBCs from WT or LMP7-deficient mice, which showed a typical discoid form (Fig. 4B). Percoll gradient purified schizont-rich pRBCs composed of late trophozoites and schizonts, contained many spherical RBCs, indicating that in-

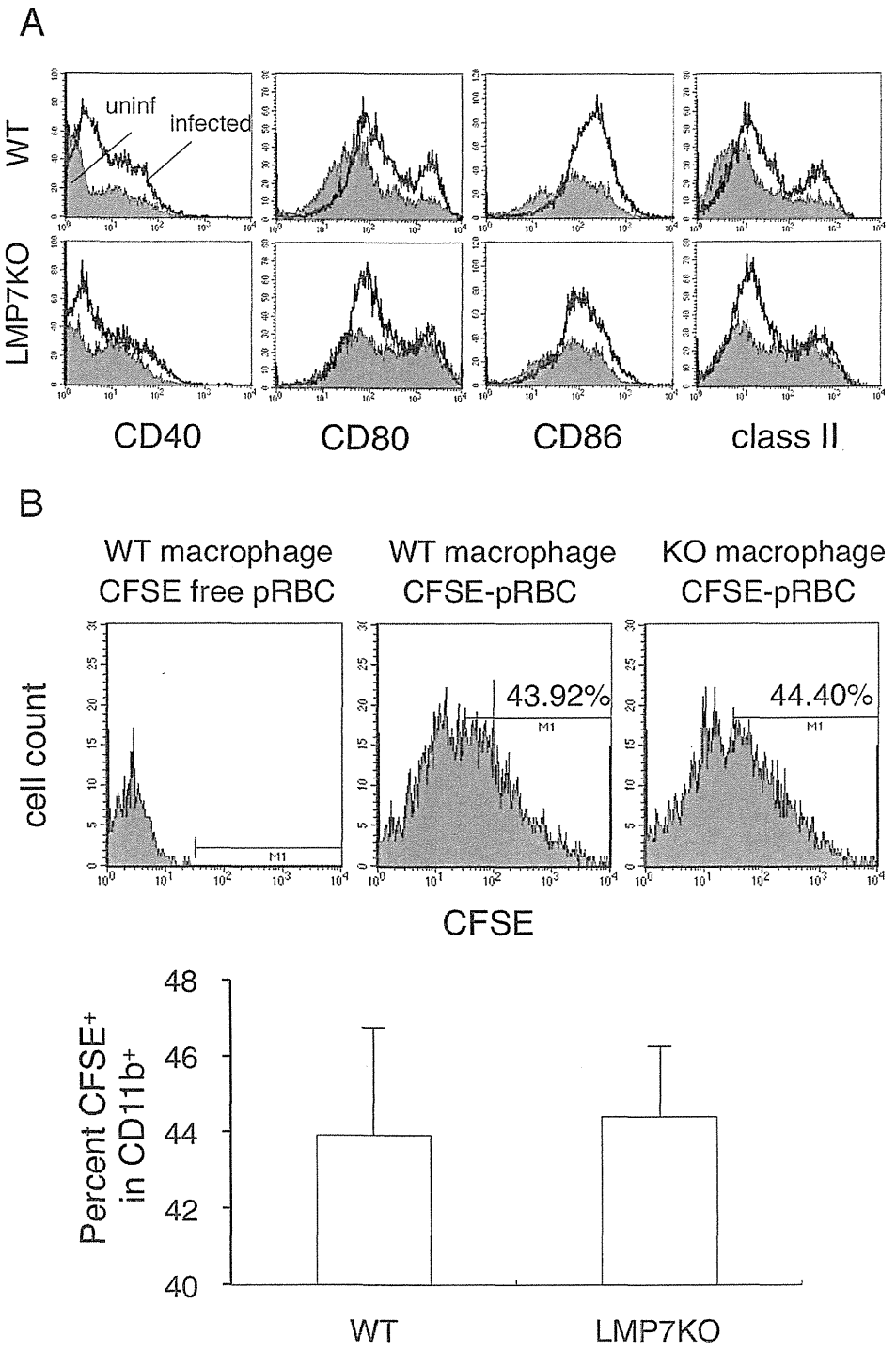


**Figure 3. Innate immune responses against *P. yoelii* in LMP7-deficient mice.** (**A**) Splenic CD11c$^+$ dendritic cells obtained from WT (upper panels) and LMP7-deficient mice (lower panels) 5 days after infection were analyzed for their expression of activation markers. Histograms show expression patterns of the indicated molecules in uninfected (shaded areas) and PyL-infected mice (bold lines). (**B**) Peritoneal macrophages from WT and LMP7-deficient mice were cultured with CFSE-labeled pRBCs prepared from WT mice for 1 hour at 1:10 ratio. After removing free RBCs by lysis with 0.83% $NH_4Cl$, macrophages were stained with PE-conjugated anti-mouse CD11b antibody before flow cytometric analyses. Histograms represent CFSE intensity of gated CD11b$^+$ macrophages. CFSE-positive cells were determined by fluorescence intensity of macrophages cultured with CFSE-free pRBCs (left panel). Numbers indicate percentage of CFSE-positive cells. Values in the bar graph represent mean ± SD of three mice, and statistical significance was not observed.
doi:10.1371/journal.pone.0059633.g003

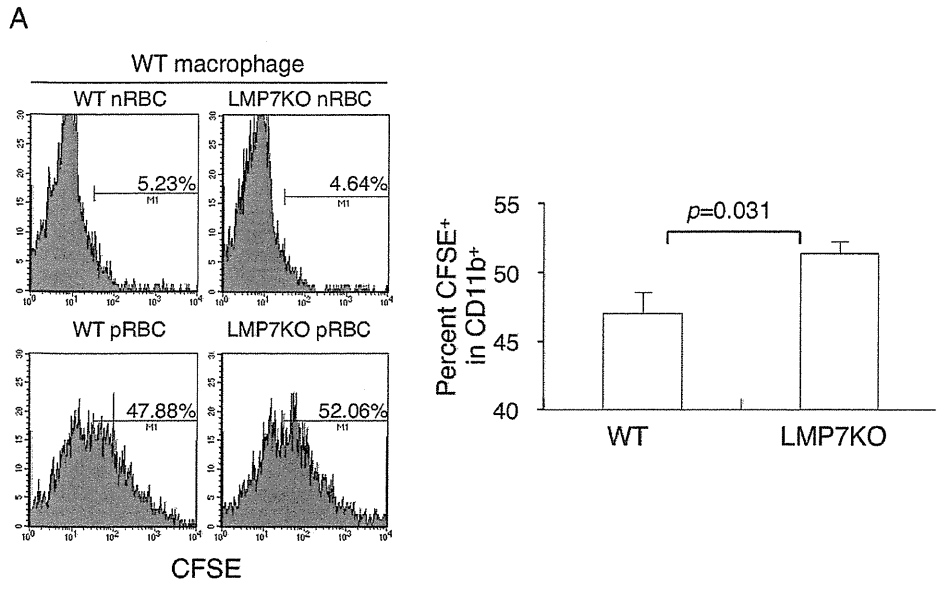
A
WT macrophage
WT nRBC
LMP7KO nRBC
5.23%
4.64%
WT pRBC
LMP7KO pRBC
47.88%
52.06%
CFSE
Percent CFSE+ in CD11b+
55
50
45
40
p=0.031
WT
LMP7KO

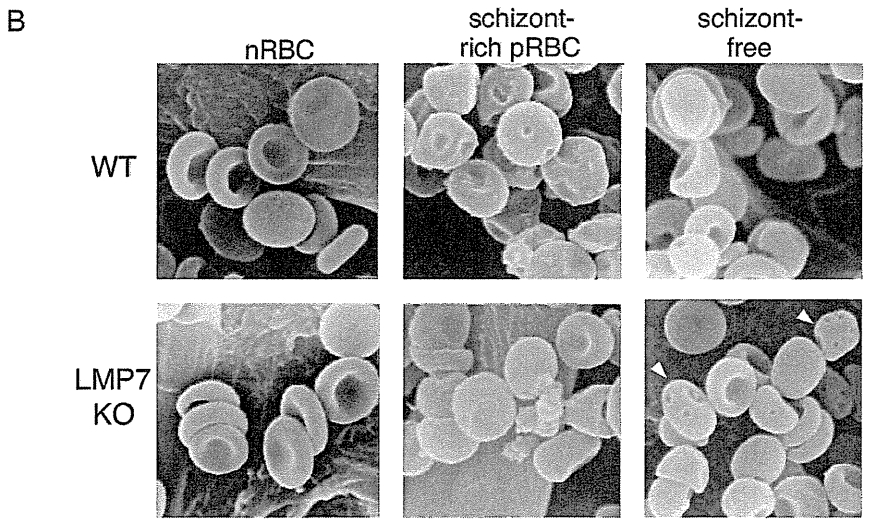
B
nRBC
schizont-rich pRBC
schizont-free
WT
LMP7 KO

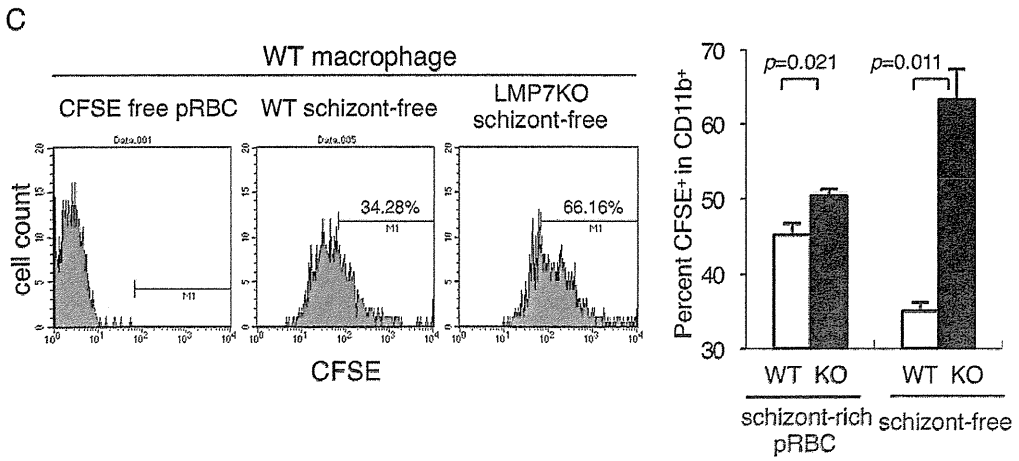
C
WT macrophage
CFSE free pRBC
WT schizont-free
LMP7KO schizont-free
cell count
34.28%
66.16%
CFSE
Percent CFSE+ in CD11b+
70
60
50
40
30
p=0.021
p=0.011
WT KO
WT KO
schizont-rich pRBC
schizont-free

**Figure 4. Susceptibility of RBCs from LMP7-deficient mice infected with PyL to phagocytosis by macrophages.** (**A**) Peritoneal macrophages obtained from WT mice were cultured with CFSE-labeled nRBCs and pRBCs prepared from WT or LMP7-deficient mice as in Fig. 3B. Phagocytosing macrophages were determined as in Fig. 3B. Values in the bar graph represent mean ± SD of three mice, and statistical significance was evaluated by Student's *t*-test. (**B**) Morphology of RBCs from uninfected mice (left panels), pRBCs containing late trophozoites and schizonts (center panels), and RBCs other than pRBCs (right panels) from WT (upper panels) or LMP7-deficient mice (lower panels) was examined by SEM. Arrowheads indicate deformed RBCs with small dimples. Scale bars = 10 μm. (**C**) Peritoneal macrophages obtained from WT mice were cultured with CFSE-labeled RBCs after removal of pRBCs prepared from WT or LMP7-deficient as in Fig. 3B except that the RBC to macrophage ratio was 100:1.
doi:10.1371/journal.pone.0059633.g004

fection with PyL altered the morphology of the RBCs. These deformations were equally observed in both WT and LMP7-deficient mice. However schizont-free RBCs, which were separated as the precipitant by Percoll gradient consisting of early trophozoites (rings) and uninfected RBCs, showed a distinct difference. RBCs from LMP7-deficient mice showed many small dimples, whereas such RBCs were rarely seen in WT mice. Quantifications based on SEM images revealed that the ratios of dimple-containing schizont-free RBCs in LMP7-deficient or WT mice were 25.33±0.19% or 4.66±2.40%, respectively (mean ± SD from 2 mice, $p = 0.05$). This morphology was not an artifact during the purification of pRBCs, because deformed RBCs were not observed in RBCs from uninfected mice processed the same way as infected mice samples.

Since schizont-free RBCs contained more deformed RBCs in LMP7-deficient mice compared with WT mice, we then analyzed phagocytosis of those RBCs by macrophages *in vitro*. As shown above, schizont-rich pRBCs from LMP7-deficient mice were phagocytosed at a greater rate than those from WT mice. Interestingly, more schizont-free RBCs from LMP7-deficient mice were phagocytosed (Fig. 4C). This remarkable difference did not reflect the proportion of ring-infected RBCs. After removal of schizont-rich pRBCs, RBC preparations from WT or LMP7-deficient mice contained 63.8% or 37.8% ring-infected RBCs, respectively. These results suggested that almost all ring-infected RBCs in LMP7-deficient were captured by macrophages, presumably resulting in the partial resistance to lethal infection with PyL in these mutant mice.

## Discussion

In this study, we analyzed the importance of LMP7 in protection against infection with malaria parasites by infecting LMP7-deficient mice with PyNL or PyL. In contrast to our expectation that the failure to activate protective $CD8^+$ T cells due to the absence of LMP7 would lead to impaired protection, LMP7-deficient mice were partially resistant to malaria. Indeed, immune responses, especially $CD8^+$ T cell responses, were less activated compared with WT mice. However, lack of LMP7 conferred resistance to malaria, overcoming the partially impaired activation of $CD8^+$ T cells. Our results demonstrate that resistance observed in LMP7-deficient mice was attributed to the higher susceptibility of pRBCs for phagocytosis by macrophages. These results do not deny the importance of $CD8^+$ T cells in protective immunity against malaria, because $CD8^+$ T cells specific for LMP7-independent epitopes could be activated [37]. Indeed, substantial numbers of $CD8^+$ T cells expressed CD69 and IFN-γ in response to malaria infection in LMP7-deficient mice (Fig. 2A, C). Furthermore, our previous studies clarified that the protective effects of $CD8^+$ T cells are due to phagocytosis by macrophages activated by an IFN-γ dependent mechanism. In the presence of strong protection during the early phase of infection due to enhanced phagocytosis, the additional effects of $CD8^+$ T cells might be difficult to observe.

Phagocytosis of pRBCs occurring in reticuloendothelial systems has been reported to be critical for the elimination of malaria parasites in various situations [38]. Attachment of pRBCs infected with *P. falciparum*, a causative agent of malignant malaria, to endothelial cells may be an escape mechanism to prevent trafficking to the spleen where phagocytosis occurs [39]. Considering these facts, it is possible that the enhanced phagocytosis is responsible for resistance of LMP7-deficient mice. As the phagocytic ability of LMP7-deficient macrophages was comparable to that of WT macrophages, the alterations of RBCs observed during infection might be important for the enhanced phagocytosis.

Under physiological conditions, macrophages in the reticuloendothelial system destroy senescent RBCs to maintain homeostasis by recognizing physical alterations in RBCs, such as lack of flexibility and deformity. Macrophages also recognize chemical and antigenic alterations. For instance, they capture "eryptotic" RBCs exposing phosphatidylserine (PS) flipped from the internal leaflet of the RBC membrane [40]. Externalization of PS is a hallmark of apoptosis in nucleated cells, which provides phagocytes with "eat-me" signals. RBCs exposing PS are also observed in iron-deficiency anemia and drug treatment enhanced phagocytosis of pRBCs during malaria, resulting in a partial protection against malaria [41,42]. Thus, we examined the exposure of PS in RBCs from LMP7-deficient mice infected with PyL. However, infection with PyL did not cause externalization of PS to the surface of RBCs in either WT or LMP7-deficient mice (data not shown).

Instead, we found that RBCs have deformations during malaria in LMP7-deficient mice. As patients with abnormal RBCs disorders such as hereditary spherocytosis suffer from splenomegaly, a hallmark of digesting abnormal RBCs and a target for physiological therapy or splenectomy [43], abnormal RBC structures could target RBCs for phagocytosis. In our study, ring-infected RBCs and uninfected RBCs other than schizont-rich RBCs showed remarkable structural changes that were highly susceptible to phagocytosis. The uptake of ring-infected pRBCs possibly disrupt the cycle of malaria parasites. The intake of small amounts of parasite-derived molecules (stimulants for innate immunity and antigens recognized by adaptive immunity) might explain the low immune responses to malaria parasites in LMP7-deficient mice. We suggest that deformation is a major cause of the higher susceptibility of pRBCs to phagocytosis followed by resistance observed in these mutants, although we could not confirm it experimentally as alterations of RBC membrane could not be artificially reproduced. Furthermore, the difference in phagocytosis could be due to other changes in the RBCs besides deformability, such as more affinity to complement on the RBCs. In addition to the susceptibility of deformed RBCs to phagocytosis, such RBCs might be refractory to invasion of merozoites. Unfortunately, this could not be evaluated because mouse malaria parasites could not be cultured *in vitro*.

Although we have not addressed how the deficiency of LMP7 led to deformed RBCs during infection, two possibilities are postulated. First, LMP7 functions in RBCs and is involved in the development of RBCs. Lack of LMP7 during the cellular development may alter membrane structures and the distribution of components responsible for intracellular homeostasis. Thus,

these resultant RBCs could not manage harmful conditions associated with malaria, such as oxidative stress [44] or physiological stress. However, previous studies have reported that RBCs only contain constitutive proteasomes, and not immune proteasomes [45,46]. We also confirmed that LMP7 is not expressed in RBCs even after infection (data not shown). Therefore, the developmental defects, if any, must occur in erythroblasts before maturation of RBCs. Second, LMP7 functions in other cell types other than RBCs, possibly including immune cells. It has been reported that inflammatory responses induce proteins associated with cytoprotection, such as stress proteins [47]. Lack of cytoprotective effects during malaria may cause RBCs to deform. However, unfortunately the higher deformability of LMP7-deficient RBCs could not be assessed because factors during infection inducing deformation are unknown. Anyway, it would be of great interest to examine membrane-associated and cytosolic proteins of RBCs in LMP7-deficient mice. Such approaches exploring these unexpected results may reveal novel host-parasite relationships in malaria.

## Acknowledgments

We thank A. Takade and M. Sano for technical support.

## Author Contributions

Conceived and designed the experiments: XD HH. Performed the experiments: XD TI BC. Analyzed the data: XD TI KH KS MH TT HO CS. Contributed reagents/materials/analysis tools: LT. Wrote the paper: XD HH.

## References


1. Rock KL, Gramm C, Rothstein L, Clark K, Stein R, et al. (1994) Inhibitors of the proteasome block the degradation of most cell proteins and the generation of peptides presented on MHC class I molecules. Cell 78: 761–771.
2. Coux O, Tanaka K, Goldberg AL. (1996) Structure and functions of the 20S and 26S proteasomes. Annu Rev Biochem 65: 801–847.
3. Palombella VJ, Rando OJ, Goldberg AL, Maniatis T. (1994) The ubiquitin-proteasome pathway is required for processing the NF-κB1 precursor protein and the activation of NF-κB. Cell 78: 773–785.
4. Pagano M. (1997) Cell cycle regulation by the ubiquitin pathway. Faseb J 11: 1067–1075.
5. Fujiwara T, Tanaka K, Orino E, Yoshimura T, Kumatori A, et al. (1990) Proteasomes are essential for yeast proliferation. cDNA cloning and gene disruption of two major subunits. J Biol Chem 265: 16604–16613.
6. Shimbara N, Orino E, Sone S, Ogura T, Takashina M, et al. (1992) Regulation of gene expression of proteasomes (multi-protease complexes) during growth and differentiation of human hematopoietic cells. J Biol Chem 267: 18100–18109.
7. Ichihara A, Tanaka K, Andoh T, Shimbara N. (1993) Regulation of proteasome expression in developing and transformed cells. Adv Enzyme Regul 33: 173–180.
8. Tsukahara T, Sugita H, Ishiura S. (1991) 26S multicatalytic proteinase complexes decrease during the differentiation of murine erythroleukemia cells. Biochim Biophys Acta 1079: 273–278.
9. Ebisui C, Tsujinaka T, Morimoto T, Fujita J, Ogawa A, et al. (1995) Changes of proteasomes and cathepsins activities and their expression during differentiation of C2C12 myoblasts. J Biochem 117: 1088–1094.
10. Sadoul R, Fernandez PA, Quiquerez AL, Martinou I, Maki M, et al. (1996) Involvement of the proteasome in the programmed cell death of NGF-deprived sympathetic neurons. EMBO J 15: 3845–3852.
11. Grimm LM, Goldberg AL, Poirier GG, Schwartz LM, Osborne BA. (1996) Proteasomes play an essential role in thymocyte apoptosis. EMBO J 15: 3835–3844.
12. Rock KL, York IA, Saric T, Goldberg AL. (2002) Protein degradation and the generation of MHC class I-presented peptides. Adv Immunol 80: 1–70.
13. Brown MG, Driscoll J, Monaco JJ. (1991) Structural and serological similarity of MHC-linked LMP and proteasome (multicatalytic proteinase) complexes. Nature 353: 355–357.
14. Yang Y, Waters JB, Fruh K, Peterson PA. (1992) Proteasomes are regulated by interferon gamma: implications for antigen processing. Proc Natl Acad Sci U S A 89: 4928–4932.
15. Aki M, Shimbara N, Takashina M, Akiyama K, Kagawa S. et al. (1994) Interferon-gamma induces different subunit organizations and functional diversity of proteasomes. J Biochem 115: 257–269.
16. Akiyama K, Kagawa S, Tamura T, Shimbara N, Takashina M, et al. (1994) Replacement of proteasome subunits X and Y by LMP7 and LMP2 induced by interferon-gamma for acquirement of the functional diversity responsible for antigen processing. FEBS Lett 343: 85–88.
17. Akiyama K, Yokota K, Kagawa S, Shimbara N, Tamura T. et al. (1994) cDNA cloning and interferon gamma down-regulation of proteasomal subunits X and Y. Science 265: 1231–1234.
18. Fruh K, Gossen M, Wang K, Bujard H, Peterson PA, et al. (1994) Displacement of housekeeping proteasome subunits by MHC-encoded LMPs: a newly discovered mechanism for modulating the multicatalytic proteinase complex. EMBO J 13: 3236–3244.
19. Kloetzel PM, Ossendorp F. (2004) Proteasome and peptidase function in MHC-class-I-mediated antigen presentation. Curr Opin Immunol 16: 76–81.
20. Driscoll J, Brown MG, Finley D, Monaco JJ. (1993) MHC-linked LMP gene products specifically alter peptidase activities of the proteasome. Nature 365: 262–264.
21. Gaczynska M, Rock KL, Goldberg AL. (1993) Gamma-interferon and expression of MHC genes regulate peptide hydrolysis by proteasomes. Nature 365: 264–267.
22. Sijts A, Zaiss D, Kloetzel PM. (2001) The role of the ubiquitin-proteasome pathway in MHC class I antigen processing: implications for vaccine design. Curr Mol Med 1: 665–676.
23. Griffin TA, Nandi D, Cruz M, Fehling HJ, Kaer LV. et al.(1998) Immunoproteasome assembly: cooperative incorporation of interferon gamma (IFN-γ)-inducible subunits. J Exp Med 187: 97–104.
24. Fehling HJ, Swat W, Laplace C, Kuhn R, Rajewsky K, et al. (1994) MHC class I expression in mice lacking the proteasome subunit LMP-7. Science 265: 1234–1237.
25. Duan X, Hisaeda H, Shen J, Tu L, Imai T, et al. (2006) The ubiquitin-proteasome system plays essential roles in presenting an 8-mer CTL epitope expressed in APC to corresponding $CD8^+$ T cells. Int Immunol 18: 679–687.
26. Ishii K, Hisaeda H, Duan X, Imai T, Sakai T, et al. (2006) The involvement of immunoproteasomes in induction of MHC class I-restricted immunity targeting *Toxoplasma* SAG1. Microbes Infect 8: 1045–1053.
27. Chou B, Hisaeda H, Shen J, Duan X, Imai T, et al. (2008) Critical contribution of immunoproteasomes in the induction of protective immunity against *Trypanosoma cruzi* in mice vaccinated with a plasmid encoding a CTL epitope fused to green fluorescence protein. Microbes Infect 10: 241–250.
28. Suss G, Eichmann K, Kury E, Linke A, Langhorne J. (1988). Roles of CD4- and CD8-bearing T lymphocytes in the immune response to the erythrocytic stages of *Plasmodium chabaudi*. Infect Immun 56: 3081–3088.
29. Kumar S, Good MF, Dontfraid F, Vinetz JM, Miller LH. (1989) Interdependence of $CD4^+$ T cells and malarial spleen in immunity to *Plasmodium vinckei vinckei*. Relevance to vaccine development. J Immunol 143: 2017–2023.
30. Pombo DJ, Lawrence G, Hirunpetcharat C, Rzepczyk C, Bryden M. et al. (2002) Immunity to malaria after administration of ultra-low doses of red cells infected with *Plasmodium falciparum*. Lancet 360: 610–617.
31. Good MF, Xu H, Wykes M, Engwerda CR. (2005) Development and regulation of cell-mediated immune responses to the blood stages of malaria: implications for vaccine research. Annu Rev Immunol 23: 69–99.
32. Lundie RJ, de Koning-Ward TF, Davey GM, Nie CQ, Hansen DS, et al. (2008) Blood-stage Plasmodium infection induces $CD8^+$ T lymphocytes to parasite-expressed antigens, largely regulated by $CD8\alpha^+$ dendritic cells. Proc Natl Acad Sci U S A 105: 14509–14514.
33. Miyakoda M, Kimura D, Yuda M, Chinzei Y, Shibata Y, et al. (2008) Malaria-specific and nonspecific activation of $CD8^+$ T cells during blood stage of *Plasmodium berghei* infection. J Immunol 181: 1420–1428.
34. Belnoue E, Kayibanda M, Vigario AM, Deschemin JC, van Rooijen N, et al. (2002) On the pathogenic role of brain-sequestered $\alpha\beta$ $CD8^+$ T cells in experimental cerebral malaria. J Immunol 169: 6369–6375.
35. Imai T, Shen J, Chou B, Duan X, Tu L, Tetsutani K, et al. (2010) Involvement of $CD8^+$ T cells in protective immunity against murine blood-stage infection with *Plasmodium yoelii* 17XL strain. Eur J Immunol 40: 1053–1061.
36. Tosta CE, Sedegah M, Henderson DC, Wedderburn N. (1980) *Plasmodium yoelii* and *Plasmodium berghei*: isolation of infected erythrocytes from blood by colloidal silica gradient centrifugation. Exp Parasitol 50: 7–15.
37. Nussbaum AK, Rodriguez-Carreno MP, Benning N, Botten J, Whitton JL. (2005) Immunoproteasome-deficient mice mount largely normal $CD8^+$ T cell responses to lymphocytic choriomeningitis virus infection and DNA vaccination. J Immunol 175: 1153–1160.
38. Stevenson MM, Ghadirian E, Phillips NC, Rae D, Podoba JE. (1989) Role of mononuclear phagocytes in elimination of *Plasmodium chabaudi* AS infection. Parasite Immunol 11: 529–544.
39. Couper KN, Blount DG, Hafalla JC, van Rooijen N, de Souza JB. et al. (2007) Macrophage-mediated but gamma interferon-independent innate immune responses control the primary wave of *Plasmodium yoelii* parasitemia. Infect Immun 75: 5806–5818.
40. Miller LH, Baruch DI, Marsh K, and Doumbo OK. (2002) The pathogenic basis of malaria. Nature 415: 673–679.

41. Moriya-Matsuzaki C, Tu L, Ishida H, Imai T, Suzue K, et al. (2011) A critical role for phagocytosis in resistance to malaria in iron-deficient mice. Eur J Immunol 41: 1365–1375.
42. Koka S, Lang C, Boini KM, Bobbala D, Huber SM, et al. (2008) Influence of chlorpromazine on eryptosis, parasitemia and survival of *Plasmodium berghei* infected mice. Cell Physiol Biochem 22: 261–268.
43. Casale M, Perrotta S. (2011) Splenectomy for hereditary sperocytosis: complete, partial or not at all? Expert Rev Hematol 4: 627–635.
44. Becker K, Tilley L, Vennerstrom JL, Roberts D, Rogerson S, et al. (2004) Oxidative stress in malaria parasite-infected erythrocytes: host-parasite interaction. Int J Parasitol 34: 163–189.
45. Froment C, Uttenweiler-Joseph S, Bousquet-Dubouch MP, Matondo M, Borges JP, et al. (2005) A quantitative proteomic approach using two-dimensional gel electrophoresis and isotope-coded affinity tag labeling for studying human 20S proteasome heterogeneity. Proteomics 5: 2351–2363.
46. Zoeger A, Blau M, Egerer K, Feist E, Dahlmann B. (2006) Circulating proteasomes are functional and have a subtype pattern distinct from 20S proteasomes in major blood cells. Clin Chem 52: 2079–2086.
47. Lee IT, Wang SW, Lee CW, Chang CC, Lin CC, Luo SF, Yang CM. (2008) Lipoteichoic acid induces HO-1 expression via the TLR2/MyC88/c-Src/NADPH oxidase pathway and Nrf2 in human tracheal smooth muscle cells. J Immunol 181: 5098–5110.

Virus Research 177 (2013) 75–86

Contents lists available at ScienceDirect

Virus Research

journal homepage: www.elsevier.com/locate/virusres

# Characterization of burdock mottle virus, a novel member of the genus *Benyvirus*, and the identification of benyvirus-related sequences in the plant and insect genomes

Hideki Kondo[a,*], Shuichi Hirano[a], Sotaro Chiba[a], Ida Bagus Andika[b], Makoto Hirai[c], Takanori Maeda[d], Tetsuo Tamada[a,*,1]

[a] Institute of Plant Science and Resources (IPSR), Okayama University, 2-20-1, Chuo, Kurashiki 710-0046, Japan
[b] Institute of Virology and Biotechnology, Zhejiang Academy of Agricultural Sciences, Hangzhou 310021, PR China
[c] Department of Parasitology, Graduate School of Medicine, Gunma University, Maebashi 371-8511, Japan
[d] Formerly College of Bioresource Sciences, Nihon University, 1866 Kameino, Fujisawa, Kanagawa 252-8510, Japan

ARTICLE INFO

*Article history:*
Received 21 June 2013
Received in revised form 17 July 2013
Accepted 18 July 2013
Available online 30 July 2013

*Keywords:*
*Benyvirus*
Burdock mottle virus
AlkB
Paleovirology
Endogenous viral element
Transcriptome shotgun assembly

ABSTRACT

The complete nucleotide sequence of the burdock mottle virus (BdMoV) isolated from an edible burdock plant (*Arctium lappa*) in Japan has been determined. BdMoV has a bipartite genome, whose organization is similar to RNA1 and RNA2 of benyviruses, beet necrotic yellow vein virus (BNYVV), beet soil-borne mosaic virus (BSBMV), and rice stripe necrosis virus (RSNV). BdMoV RNA1 (7038 nt) contains a single open reading frame (ORF) encoding a 249-kDa polypeptide that consists of methyl-transferase, helicase, papain-like protease, AlkB-like, and RNA-dependent RNA polymerase domains. The AlkB-like domain sequence is not present in the proteins encoded by other known benyviruses, but is found in replication-associated proteins of viruses mainly belonging to the families *Alfaflexiviridae* and *Betaflexiviridae*. BdMoV RNA2 (4315 nt) contains six ORFs that are similar to those of benyviruses: these are coat protein (CP), CP readthrough, triple gene block movement and cysteine-rich proteins. Phylogenetic analyses showed that BdMoV is more closely related to BNYVV and BSBMV than to RSNV. Database searches showed that benyvirus replicase-related sequences are present in the chromosomes of a chickpea plant (*Cicer arietinum*) and a blood-sucking insect (*Rhodnius prolixus*). Some other benyvirus-related sequences are found in the transcriptome shotgun libraries of a few species of plants and a bark beetle. Our results show that BdMoV is a distinct species of the genus *Benyvirus* and that ancestral and extant benyviruses may have infected or currently infect a wide range of hosts, including plants and insects.


## 1. Introduction

Burdock mottle virus (BdMoV) was first isolated from edible burdock plants (*Arctium lappa* L.) at Soja City, Okayama Prefecture, Japan in 1970 (Inouye, 1973). Similar viruses have been found in several prefectures (i.e., Saitama, Kanagawa, Akita and Tokyo) (Yamashita et al., 2008), but they have not been reported outside of Japan. Burdock is one of the domestic root vegetable crops of Japan and has been grown for a long time. *A. lappa* is a biennial plant belonging to the *Asteraceae* (*Compositae*) family and native to the Eurosiberian region and subcosmopolitan in distribution (Lopez-Vinyallonga et al., 2011). This and allied plants have also been cultivated as a traditional medicinal herb in China and other countries (Chan et al., 2011).

Burdock is the only known natural host of BdMoV. The virus usually causes mild, chlorosis or mottling symptoms on the leaves of burdock plants. It is transmissible by mechanical inoculation of sap to several plant species, but its natural vector is unknown (Inouye, 1973). BdMoV has straight rod-shaped particles, about 250 nm (a major peak) and 380 nm (a minor peak) in length and about 17 nm in width, which are similar to the particles of viruses in the genus *Benyvirus* as well as the family *Virgaviridae*. BdMoV induces the formation of spherical electron-dense, viroplasm-like inclusion bodies in the cytoplasm of cells (Inouye, 1973; Yamashita et al., 2008). Our molecular study has shown that the genome of BdMoV is similar to that of beet necrotic yellow vein virus (BNYVV) (Hirano et al., 1999), and therefore BdMoV is a tentative species of the genus *Benyvirus* (Gilmer and Ratti, 2012; Koenig and Lesemann, 2005; Rush, 2003; Tamada, 1999; Tamada and Kondo, 2013).

* Corresponding authors. Tel.: +81 86 434 1232; fax: +81 86 434 1249.
*E-mail addresses:* hkondo@rib.okayama-u.ac.jp (H. Kondo), tyrotamada@oboe.ocn.ne.jp (T. Tamada).
[1] Current address: Kita 10, Nishi 1, 13-2-606, Sapporo, 001-0010, Japan.

0168-1702/$ – see front matter © 2013 Elsevier B.V. All rights reserved.
http://dx.doi.org/10.1016/j.virusres.2013.07.015

Benyviruses have polyadenylated, segmented plus-sense RNA genomes (2–5). Most have two segments, RNA1 and RNA2, which carry important house-keeping genes required for replication, encapsidation/assembly, viral movement/transmission and RNA silencing suppression, and satellite-like RNAs depending on virus strains, which play important roles in disease development and spread in nature (Gilmer and Ratti, 2012; Heidel et al., 1997; Lee et al., 2001). At present, the genus *Benyvirus* includes three species, *Beet necrotic yellow vein virus* (type member), *Beet soil-borne mosaic virus* and *Rice stripe necrosis virus* (Gilmer and Ratti, 2012). Taxonomically, the benyvirus differs from rod-shaped viruses belonging to the family *Virgaviridae* in replicase phylogeny, genome organization and expression strategies (Adams et al., 2009; Tamada, 1999). For example, the replicase-associated protein of benyviruses shows greater similarity to that of the viruses in the families *Togaviridae* and *Hepeviridae* than to those of other rod-shaped plant viruses (Koonin et al., 1992). Most recently, an official taxonomic proposal (TaxoProp) was submitted by Gilmer et al. (2013) to the International Committee on the Taxonomy of Viruses (ICTV) requesting the creation of the new family *Benyviridae* that contains a new species *Burdock mottle virus* in the genus *Benyvirus*.

BNYVV has spread to most of sugar beet growing areas worldwide since first found in Italy in the 1950s, but its origin is suggested to be in East Asia (Chiba et al., 2011a). Beet soil-borne mosaic virus (BSBMV) occurs in almost all the major sugar beet growing regions of the United States (Rush, 2003). Both viruses have similarly limited host ranges and are vectored by *Polymyxa betae* (Plasmodiophoraceae, a fungoid protist) (Rush, 2003). Rice stripe necrosis virus (RSNV) occurs in the Ivory Coast in Africa (Louvel and Bidaux, 1977) and in South and Central America (Morales et al., 1999). RSNV is transmitted by *Polymyxa graminis* (Morales et al., 1999). Furthermore, two benyvirus-related rod-shaped viruses are known: Nicotiana velutina mosaic virus (NVMV) that was isolated from *Nicotiana velutina* plants in Australia having a bipartite genome (Randles and Rohde, 1990) and Chara australis virus (CAV) that was isolated from fresh water algae (*Chara australis*) in Australia having a monopartite genome, whose replicase is most closely related to that of benyviruses (Gibbs et al., 2011). This implies wide distribution of benyvirus-like species in various eukaryotic organisms.

Recently, the presence of several non-retroviral RNA virus sequences (NRVSs, syn. endogenous virus elements) related to plus-sense RNA viruses in host genomes. This includes some members of four plant virus genera *Citrivirus* (family *Betaflexiviridae*), *Tobamovirus* (family *Virgaviridae*), *Potyvirus* (family *Potyviridae*) and *Cilevirus* (unassigned family), one insect virus genus *Flavivirus* (family *Flaviviridae*) (Chiba et al., 2011b; Crochu et al., 2004; Cui and Holmes, 2012; Katzourakis and Gifford, 2010; Tanne and Sela, 2005). Examples of NRVSs endogenization extend to minus-sense and double-stranded RNA viruses (Chiba et al., 2011b; Horie et al., 2010; Liu et al., 2010; Katzourakis and Gifford, 2010; Kondo et al., 2013; Taylor and Bruenn, 2009). It is anticipated that a similar approach allows detection of benyvirus-like sequences in eukaryotes not reported to be their hosts.

In this study, we compared the complete nucleotide sequence of BdMoV to genomes of other viruses. Our analyses suggest that BdMoV is a new member of the *Benyvirus* genus with a bipartite genome. Bioinformatic analyses led to the identification of benyvirus replicase-related sequences in plant and insect chromosomes, which suggested that the ancient benyvirus sequences have been integrated as endogenous virus-like elements into their genomes. We also found some other benyvirus-related sequences in the transcriptome shotgun libraries from plants and insects. These data suggest that benyviruses and their related viruses may have been distributed in a wide range of hosts since ancient times.

## 2. Materials and methods

### 2.1. Virus isolate, propagation and inoculations

The S isolate of BdMoV originated from burdock leaves that were collected from a field in Soja, near Kurashiki, in 1970 (Inouye, 1973). This virus was propagated in *Chenopodium quinoa* leaves in glasshouses. Locally infected leaves of *C. quinoa* were harvested approximately 1–2 weeks after inoculation and stored at −80 °C until used.

Foliar rub-inoculation and root vector inoculation using *P. betae* were conducted as described previously (Rahim et al., 2007; Tamada, 2007).

### 2.2. Virus purification and electron microscopy

Virus particles were purified from mechanically infected leaves of *C. quinoa*. The virus-infected leaves were homogenized in 0.5 M borate–HCl (pH 8.0), containing 0.1% thioglycolic acid, 1 mM phenylmethylsulfonylfluoride, 20 mM sodium iodoacetate, and 20 mM $Na_2$-EDTA. The extract was filtrated through cheesecloth and clarified by 8.5% (w/v) *n*-butanol. After low speed centrifugation, 1% Triton X-100 (w/v) was added to the supernatant, and the virus was precipitated by adding 4% PEG6000. The preparation was resuspended in 0.5 M borate buffer (pH 8.0) and concentrated by ultracentrifugation. The resulting pellets were resuspended in 0.01 M phosphate buffer (pH 7.0) and further purified through a sucrose-cesium chloride gradient. The light-scattering bands were collected from the gradient and pelleted by ultracentrifugation. To obtain electron micrograph of BdMoV virions, purified preparations were negatively stained with 2% uranyl acetate and observed in a Hitachi model H-7100 transmission electron microscope (Hitachi, Tokyo, Japan).

### 2.3. Electrophoretic analysis of viral RNA

Viral RNA extraction from the purified virion and poly(A)-positive RNA fractionation were conducted as described previously (Andika et al., 2006; Kondo et al., 2009). Viral RNAs were separated on 1.4% agarose horizontal submarine gels in MOPS/EDTA buffer (pH 7.0) containing 0.22 M formaldehyde. Virion RNAs from Dendrobium mosaic virus-Japanese strain (DeMV-J, an unassigned potyvirus) were used for a poly(A)-positive RNA control and from cucumber mosaic virus Y strain (CMV-Y, a cucumovirus) and tobacco mosaic virus OM strain (TMV-OM, a tobamovirus) for poly(A)-negative controls.

### 2.4. SDS-PAGE and Western blot analyses

SDS-PAGE and Western blot analyses were conducted as described previously (Kondo et al., 2009). A rabbit antisera to BdMoV virions was used for immunodetection (Maeda et al., 1996).

### 2.5. cDNA synthesis and cloning

BdMoV cDNAs were synthesized using cDNA Synthesis Module (Amersham Pharmacia Biotech, Buckinghamshire, UK) primed with random hexanucleotides or a synthetic oligonucleotide $(dT)_{18}$ with a *Not*I site. The double-stranded cDNAs were inserted into the *Eco*RV site of pZErO™-2 (Invitrogen, San Diego, CA, USA). The plasmids were introduced into competent *Escherichia coli* strain TOP 10F′ (Invitrogen). For cloning of the 5′ terminal regions of both RNA1 and RNA2, 5′ RACE (rapid amplification of cDNA ends) was performed according to the methods of Kondo et al. (2006). The sequences of the primers used in the BdMoV genome analysis are available upon request.

### 2.6. Plant and insect materials and PCR amplification

The blood-sucking bug (*Rhodnius prolixus*) individuals, which were kindly provided by H. Kanuka of Jikei University School of Medicine (Tokyo, Japan), and the commercially available seeds of chickpeas (*Cicer arietinum* cv. unknown) were used. Total genomic DNA was purified using the DNeasy® Blood and Tissue Kit (Qiagen, Hilden, Germany) according to the manufacturer's instructions. Purified DNA solutions (TE buffer) were stored at 4 °C until use. To amplify the virus-like sequence fragments from these DNA samples by PCR, primer pairs were designed based on the virus-related sequences and their flanking sequences (Supplementary Table S1 and data not shown).

### 2.7. Nucleotide sequencing and sequence analysis

Nucleotide sequences of selected clones were determined by dideoxy chain termination using Applied Biosystems 377 or 3100 DNA sequencer (Applied Biosystems, Foster City, CA). Sequence data were assembled and analyzed by Auto Assembler™ DNA Sequence Assembly Software (Applied Biosystems), and GENETYX-MAC/ATSQ (GENETYX Co., Tokyo, Japan) and Enzyme X version 3 (http://nucleobytes.com/index.php/enzymex). Sequence similarities among viruses were searched using the BLAST program available from the National Center for Biotechnology Information (NCBI).

BLAST (tblastn) searches were conducted against genome sequence databases available from the NCBI (nucleotide collection, nr/nt; genome survey sequences, GSS; high-throughput genomic sequences, HTGS; whole-genome shotgun contigs, WGS; non-human, non-mouse expressed sequence tags, EST; transcriptome shotgun assembly, TSA, others). For the searches, we used BdMoV and other benyviruses as queries. Plant and insect genome sequences that matched viral peptides with *E*-values of <0.01 were extracted. Transposable element sequences were detected using the Censor provided by Genetic Information Research Institute, USA (http://www.girinst.org/censor/index.php) (Kohany et al., 2006).

Phylogenetic tree construction was based on a maximum-likelihood (ML) method as described previously with minor modification (Kondo et al., 2013). Multiple alignments of amino acid (aa) sequences were conducted using MAFFT ver 7 under the default parameters (http://mafft.cbrc.jp/alignment/server/phylogeny.html) (Katoh and Toh, 2008). The program GapStreeze was used to remove columns that contained gaps from the alignment (Los Alamos HIV Sequence Database; http://www.hiv.lanl.gov/content/sequence/GAPSTREEZE/gap.html). Selection of the best-fit model for a data set was performed using ProtTest 2.4 (Abascal et al., 2005) based on the Akaike information criterion (AIC). ML trees were constructed by PhyML 3.0 using the appropriate substitution mode (http://www.atgc-montpellier.fr/phyml/) (Guindon et al., 2010). The branch support values were estimated by the approximate likelihood ratio test (aLRT) with a Shimodaira–Hasegawa-like (SH-like) algorithm (Anisimova and Gascuel, 2006). The obtained trees were visualized using FigTree v1.3.1 software (http://tree.bio.ed.ac.uk/software/).

## 3. Results

### 3.1. Biological and chemical properties of BdMoV

Inouye (1973) reported that BdMoV could infect 10 of 40 species from 10 families; systemic infection in burdock, *C. quinoa*, *Chenopodium murale*, *Nicotiana clevelandii* and *Nicotiana rustica*, and local infection in *Chenopodium amaranticolor*, *Beta vulgaris*, *Spinacia oleracea*, *Cucumis sativus* and *Tetragonia expansa*. Our additional inoculation tests showed that *Nicotiana benthamiana* is a systemic host, while *Gomphrena globosa* is a local lesion host. BdMoV also produced only local chlorotic lesions (no systemic infection) on *Beta macrocarpa* and *B. vulgaris* subsp. *maritima* M8 plants (data not shown) that are the systemic hosts of BNYVV (Tamada, 2007). BdMoV-infected *N. benthamiana* plants showed mild mosaic or mottle symptoms with slight leaf distortion (data not shown), which is similar to those caused by BNYVV (Rahim et al., 2007).

We attempted to allow *P. betae* to acquire BdMoV from the roots of *N. benthamiana* plants systemically infected by foliar rub-inoculation and to transmit to healthy *N. benthamiana* and *C. quinoa* plants. As a result, *P. betae* failed to transmit the virus to these plants (data not shown). In contrast, *P. betae* could transmit BNYVV, a positive control, from virus-infected *N. benthamiana* roots to healthy counterparts.

BdMoV particles are about 17 nm in diameter, with two predominant lengths of 250 nm and 380 nm (Inouye, 1973). Purified preparations contained straight rod-shaped virions of 250-nm long (Fig. 1A, asterisks) and mostly aggregated end-to-end (Fig. 1A). The purified BdMoV particles were transmitted by leaf-rub inoculation, and induced a mild systemic mottle symptom in burdock and typical chlorotic spots on *C. quinoa*-inoculated leaves, respectively (Fig. 1B and C). Electrophoresis of RNAs prepared from the purified particles showed two species of single-stranded RNA, designated RNA1 (7 kb) and RNA2 (4 kb) (Fig. 1D, left panel, BdMoV and data not shown). Both RNA1 and 2 were found in the poly(A)-positive fraction, which suggests that BdMoV RNAs have a poly(A) tail, as the positive control, DeMV-J (Fig. 1D, right panel, BdMoV and DeMV-J). In SDS-PAGE from purified virus particles, a single major polypeptide (CP) of approximately 23 kDa was detected (Fig. 1E, left panel, Virions). Western blot analysis showed that the CP protein (from the purified preparation) strongly reacted with an antiserum to the BdMoV virion (Fig. 1E, right panel, Virions). CP was detected in protein extracts from BdMoV-infected *C. quinoa* leaves, but not in those from healthy leaves (Fig. 1E, right panel, Infected and Mock). It is noted that a protein with higher molecular weight (HMW, ~60 kDa) reacted with the BdMoV antiserum (Fig. 1E, right panel, BdMoV-Infected).

### 3.2. Nucleotide sequence of the BdMoV genome

Two independent sequence contigs (RNA1 and RNA2) were obtained from the assembly of a random cDNA library of BdMoV RNAs (data not shown). Their 5′ termini were determined by 5′ RACE. The total number of nucleotide of BdMoV RNA1 and RNA2 is 7038 nt (Genebank accession AB818898) and 4315 nt (Genebank accession AB818899), respectively excluding the 3′-terminal poly(A) tail. Computer-assisted sequence analyses identified that there were only large open reading frames (ORFs) in 5′-to-3′ orientation (positive strand) of the RNA1 and RNA2 cDNAs (Fig. 2 and see below for details). The BdMoV RNA1 sequence contains one large ORF encoding a polypeptide of 249 kDa (replicase; p249) (Fig. 2). The 5′ and 3′ non-coding regions of RNA1 are 151 and 233 nt, respectively excluding the 3′-poly(A). BdMoV RNA2 contains six ORFs and the 5′ and 3′ non-coding regions of RNA2 are 147 and 227 nt, respectively (Fig. 2). The first 8 nt (AAAUUCAU) at the 5′-terminal sequence of both segments are identical (Supplementary Fig. S1A). The 3′-terminal of two segments share high similarity (85% identical, Supplementary Fig. S1B). In particular, both the 3′-proximal 70 nt of BdMoV and BNYVV RNAs can be folded into a possibly similar stem-loop structure (data not shown) (Richards and Tamada, 1992).

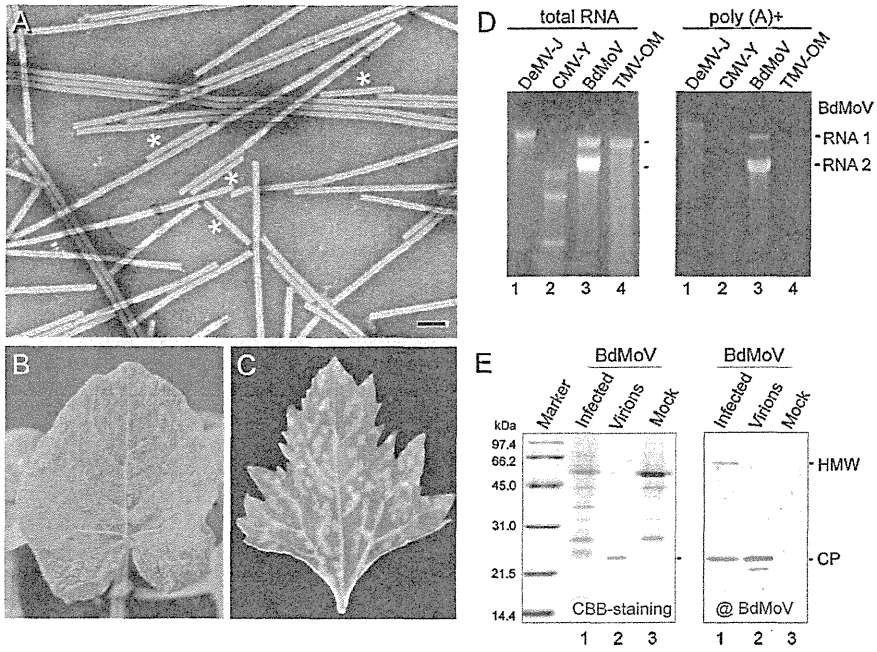


**Fig. 1.** (A) Electron micrographs of the purified virus particles. Samples were stained in uranyl acetate. The bar represents 100 nm. Asterisks: particle about 250 nm in length. (B and C) Symptoms in burdock (B) and *Chenopodium quinoa* (C) infected with BdMoV. (D) Denaturing gel electrophoretic analysis of the BdMoV RNAs before and after poly(A)$^+$ fractionation. Each sample was resolved on 1.2% agarose gels followed by ethidium bromide staining. Lane 1: Dendrobium mosaic virus Japanese isolate (DeMV-J); lane 2: cucumber mosaic virus-Y (CMV-Y); lane 3: BdMoV; and lane 4: tobacco mosaic virus-OM (TMV-OM). The positions of the BdMoV RNAs 1 and 2 are indicated on the right. (E) SDS-PAGE and Western blot analyses of partially purified preparations. Each sample was resolved on 12% SDS-PAGE gels followed by Coomassie brilliant blue-R250 staining (CBB-staining, left panel). The resolved proteins were transferred to nitrocellulose and reacted with rabbit polyclonal antiserum to BdMoV (@BdMoV, right panel). Lane 1: total proteins of the BdMoV-infected *C. quinoa* leaf (Infected); lane 2: BdMoV virion; and lane 3: total proteins of the mock plant leaf (Mock). The positions of the CP and high-molecular-weight protein (HMW, ~60 kDa) are indicated on the right. The positions of the marker proteins are shown on the left.

### 3.3. *RNA1 encoded protein*

BdMoV RNA1 encodes a single protein with an estimated molecular weight of 249-kDa and a putative replicase function (Fig. 2). This replicase-associated protein contains five domains; methyltransferase (MTR), RNA helicase (HEL), papain-like proteinase (Pro), AlkB-like protein (AlkB) and RNA-dependent RNA polymerase (RdRp) (Fig. 2, Supplementary Fig. S2A). Except for the AlkB-like, those domains are similarly found in benyvirus replicases (see below): BNYVV p237, BSBMV 239 kDa and RSNV 236 kDa proteins (Bouzoubaa et al., 1987; Lee et al., 2001; Lozano and Morales, 2009; Saito et al., 1996). In fact, a BLAST search using the deduced aa sequence of BdMoV 249 kDa protein for the NCBI Conserved Domain Database revealed HEL (Viral_helicase [pfam01443]; *E*-value = $1e^{-28}$), Pro (Peptidase_C36 [pfam05415]; *E*-value = $1e^{-15}$) and RdRp (RdRP_2 [pfam00978]; *E*-value = $5e^{-11}$) domains and no MTR or AlkB-like protein domains (Fig. 2).

A phylogenetic (ML) tree based on the three concatenated domain sequences (MTR, HEL and RdRp) for benyviruses and representative viruses of different families is shown in Fig. 3A.

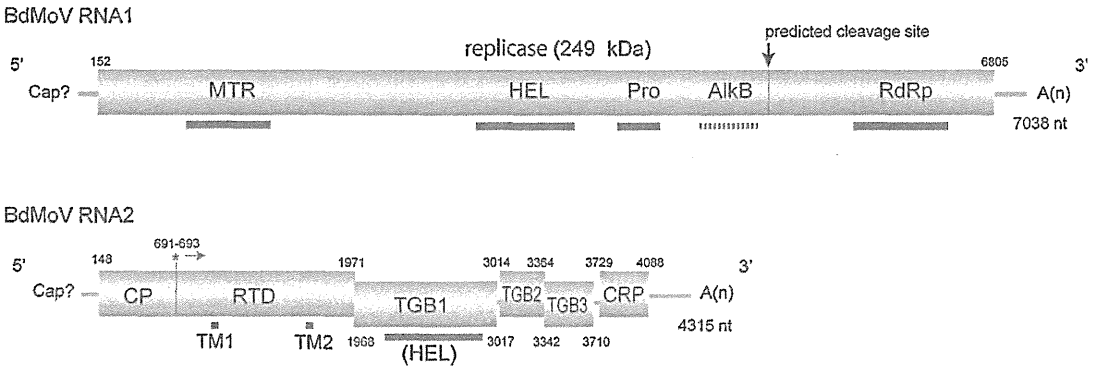


**Fig. 2.** Genomic organization of BdMoV. RNA1 contains a single open reading frame (ORF, rectangle). The methyltransferase (MTF), RNA helicase (HEL), papain-like protease (Pro) and RNA-dependent RNA polymerase (RdRp) domains are indicated by bold bars on the 249-kDa replicase. The AlkB-like domain is shown by a dashed bar. The arrowhead shows the location of the putative cleavage site for polyprotein. RNA2 contains six ORFs. The coat protein (CP; 20 kDa) cistron is separated from a long in-phase ORF (46-kDa readthrough domain, RTD) by a single amber termination codon (star, UAG), which permits expression of a 66-kDa fusion protein. The third to fifth ORFs (38, 12 and 13 kDa, respectively) are presumably associated with viral spreading since they are similar to triple gene block (TGB). The HEL motif on the 38-kDa protein is indicated by the bold bar. The sixth ORF (13 kDa) on RNA2 is similar to the cysteine-rich protein (CRP) of benyviruses. The Cap? represents the putative 5'-cap structure and the A(n) indicates the 3' poly(A) tail. Comparisons of the flanking leaky UAG (amber, 691–693) codon in BdMoV with the corresponding sequences in benyviruses revealed that these are mostly similar and a possible stem–loop-like structure at 3'-adjacent to the UAG was conserved (Firth et al., 2011) (see Supplementary Fig. S1C). The position (in nucleotides) of the start and stop codons of each predicted ORF are shown.

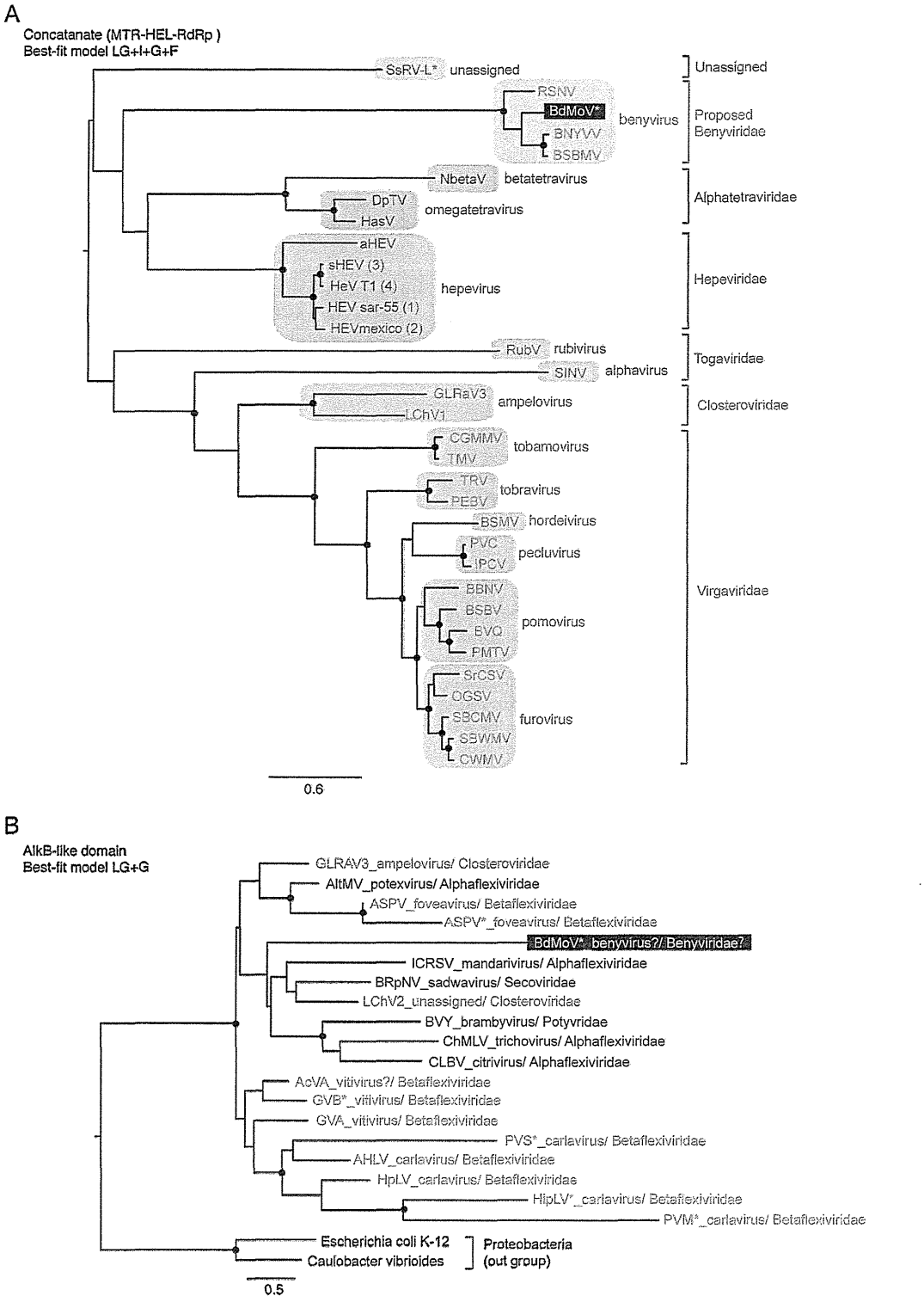


**Fig. 3.** (A) Phylogenetic (ML) tree calculated from the concatenated amino acid sequences of three domains (Met–Hel–RdRp) in the putative replicase proteins of BdMoV and benyviruses together with some other related plant, insect and animal RNA viruses. Asterisks show the unassigned viruses. (B) ML tree of BdMoV and selected viral AlkB-like domains rooted by the proteobacteria outgroup. Putatively dysfunctional AlkBs are indicated with an asterisk (van den Born et al., 2008). For both tree constructions, the alignments of the amino acid sequences were generated with MAFFT (Supplementary Fig. S3A and B). The trees were constructed by the ML method using PhyML 3.0. The branch support values were estimated using the approximate likelihood ratio test (aLRT) with a Shimodaira–Hasegawa-like (SH-like) algorithm (only values greater than 0.9 are shown as filled circles). The scale bars represent the amino acid distances. The sequences of the three replicase-associated and AlkB-like domains of RNA viruses were obtained from the EMBL/DDBJ/GenBank database and are listed in Supplementary Table S2.

It is clear that BdMoV is included within the cluster of three benyviruses: BNYVV, BSBMV and RSNV. This benyvirus cluster is more related to clades of hepeviruses (*Hepeviridae*), omegatetraviruses and betatetravirus (*Tetraviridae*), and a novel mycovirus (Sclerotinia sclerotiorum RNA virus L, SsRV-L) than to rubivirus and alphavirus (*Togaviridae*), and other rod-shaped viruses belonging to the *Virgaviridae* and filamentous viruses (*Closteroviridae*) associated with plant hosts. A similar topology was found in ML trees constructed with individuals of above three motifs of BdMoV and selected viruses (data not shown).

As shown in Table 1, three distinct domains (MTR, HEL and RdRp) of the BdMoV replicase are 44–81% identical to the corresponding domains of three other benyviruses, and 30–35% identical to those of CAV excluding its MTR domain which is undetermined (Gibbs et al., 2011). The BdMoV Pro domain shows 33–44% identity with that of three benyviruses.

When compared with other viruses, BdMoV HEL domain shares modest level of identity with the two insect omegatetraviruses, Dendrolimus punctatus virus (DpTV, GeneBank accession AAT27317; *E*-value = $3e^{-25}$, identity = 25%) and Helicoverpa armigera stunt virus (GeneBank accession AAC98529; *E*-value = $3e^{-4}$, identity = 24%). This domain also shows aa sequence similarities (GeneBank accession AER13447; *E*-value = $2e^{-9}$, identity = 27%) with the TGB1 helicase of hibiscus green spot virus, which is a novel bacilliform virus distantly related to the member of the genus *Cilevirus* (unassigned family). Furthermore, the BdMoV RdRp domain shares 30% identity (*E*-value = $6e^{-12}$) with hepatitis E virus (HEV, family *Hepeviridae*), while it shows even or lower identities (*E*-value = 0.008–$5e^{-10}$, identities = 23–30%) with some members of the *Virgaviridae* and *Closteroviridae* (data not shown).

Interestingly, the BdMoV 249-kDa replicase contains an additional sequence, that is the so-called AlkB-like domain, which is a member of the 2-oxoglutarate- and Fe(II)-dependent oxygenase superfamily (Bratlie and Drablos, 2005; van den Born et al., 2008). This domain is located between the Pro and RdRp domains (aa positions 1495 to 1630) in the BdMoV replicase, where no corresponding motif is present in the replicases of three other benyviruses (Fig. 2, Supplementary Fig. S2A). Due to the presence of this domain and its surrounding sequences, the size of the BdMoV replicase is slightly larger than that of other benyviruses.

AlkB-like protein genes are widespread in eukaryotes and bacteria, and have also been identified in replication-associated proteins of numerous viruses largely belonging to the families *Betaflexiviridae* and *Alfaflexiviridae* (Bratlie and Drablos, 2005; Martelli et al., 2007). BLAST analysis shows that BdMoV AlkB-like regions represent a weak similarity to other AlkB genes; e.g., viral AlkB-like protein sequences from the American hop latent virus (genus *Carlavirus*, family *Betaflexiviridae*) (GeneBank accession AFI61519; *E*-value = 0.005, identity = 29%, query cover = 80%) and actinidia virus A (genus *Vitivirus*, family *Betaflexiviridae*) (GeneBank accession AET36885; *E*-value = 0.008, identity = 28%, query cover = 99%) and AlkB protein of proteobacteria *Shewanella woodyi* ATCC 51908 (GeneBank accession ACA87888; *E*-value = 0.015, identity = 27%, query cover = 80%).

The ML phylogenetic tree based on the BdMoV AlkB and selected AlkB-like sequences from plant viruses showed that the BdMoV sequence forms a clade with several other viral AlkBs (Fig. 3B). However, the tree topology did not reflect the viral phylogeny based on their replication-associated protein as described previously (van den Born et al., 2008). In the aa alignment of the selected AlkBs, the BdMoV AlkB-like sequence appeared to contain a less-conserved region in the middle (Supplementary Fig. S4). This feature was similarly observed in AlkB sequences of carlaviruses such as potato virus M, potato virus S and hippeastrum latent virus, and some other betaflexiviruses, although evolutional implications are unclear (Bratlie and Drablos, 2005; van den Born et al., 2008).

### 3.4. RNA2 encoded proteins

BdMoV RNA2 encodes a 20-kDa coat protein (CP) at its 5′ extremity, containing the conserved CP motif (TMV_coat [pfam00721]; *E*-value = $7e^{-10}$), followed by an in-phase ~46-kDa ORF (readthrough domain, RTD) which is presumably expressed by translational readthrough of the CP cistron amber termination codon (66-kDa CP-RT protein) (Fig. 2). Three following partially overlapping ORFs, encoding the proteins of 38 kDa (p38), 12 kDa (p12) and 13 kDa (p13), which form a cassette of cell-to-cell movement protein-specifying genes known as triple gene block (TGB) (Fig. 2). BdMoV TGB1 and TGB2 proteins possess the RNA helicase (pfam01443; *E*-value = $1e^{-22}$) and the plant viral movement protein (Plant_vir_prot [pfam01307]; *E*-value = $1e^{-16}$) motifs, respectively. The 3′-proximal ORF encodes a cysteine-rich 13-kDa protein (p13 CRP) (Fig. 2). Accordingly, the genome organization of BdMoV RNA2 is quite similar to that of benyvirus RNA2 (Bouzoubaa et al., 1986; Lee et al., 2001; Lozano and Morales, 2009; Saito et al., 1996).

The phylogenetic (ML) analyses of aa sequences of CPs from BdMoV and other related rod-shaped plant viruses clearly demonstrate that BdMoV is clustered with benyviruses which are more closely related to the furoviruses and pomoviruses than to pecluviruses and hordeiviruses (Fig. 4A). BdMoV CP has 31–39% identity to benyvirus CPs (Table 1). The CP of CAV is closely related to those of tobamoviruses, although the CAV replicase is more similar to benyvirus replicase (Gibbs et al., 2011) (Fig. 4A).

As shown in Table 1, the aa sequence similarities of benyviruses in the RT domain are not very large. The aa sequence alignment showed that the BdMoV RT domain was somewhat different from those of BNYVV and BSBMV (Supplementary Fig. S2B, CP-RT), but their hydropathy profiles are similar to each other (data not shown), suggesting a structural homology. There are two hydrophobic regions at both the N- and C-termini of the RT domain. These are

**Table 1**
Comparisons of amino acid sequence identity of the viral proteins or motif domains between BdMoV and related virus sequences available in the GenBank database.

| Virus[a] | RNA1 (replicase, 249 kDa protein) | | | | | RNA2 | | | | | |
|---|---|---|---|---|---|---|---|---|---|---|---|
| | MTR | HEL | Pro | RdRp | CP | RTD | TGB1 | TGB2 | TGB3 | CRP | RefSeq/Accession no. |
| BNYVV | 62[b] | 67 | 44 | 81 | 39 | 24 | 48 | 48 | 38[8] | nh[c] | NC_003514, NC_003515 |
| BSBMV | 58 | 67 | 42 | 80 | 35 | 31 | 46 | 39 | 34 | nh | NC_003506, NC_003503 |
| RNSV | 44 | 66 | 33 | 76 | 31 | nh | 42 | 43 | nh | nh | EU099844, EU099845 |
| NVMV* | ud[c] | ud | ud? | ud | nh | –? | 32 | 38 | nh | –? | D00906 |
| CAV* | ud | 30 | –[c] | 35 | nh | – | – | – | – | – | JF824737 |
| HEV | nh | nh | nh | 30 | nh | – | – | – | – | – | M74506 |
| DpTV | nh | 25 | –? | 25 | nh | – | – | – | – | – | NC_005898, NC_005899 |

[a] Unassigned viruses are indicated by their abbreviation with asterisks (see Supplementary Table S2).
[b] The percent of amino acid sequence identity in the sequence comparison analysis is shown. Each scores are calculated by the BLASTp with the expect value significance cut-off below 10 (the default parameter setting).
[c] nh, no hit against the corresponding target; ud, undetermined; –, not present.

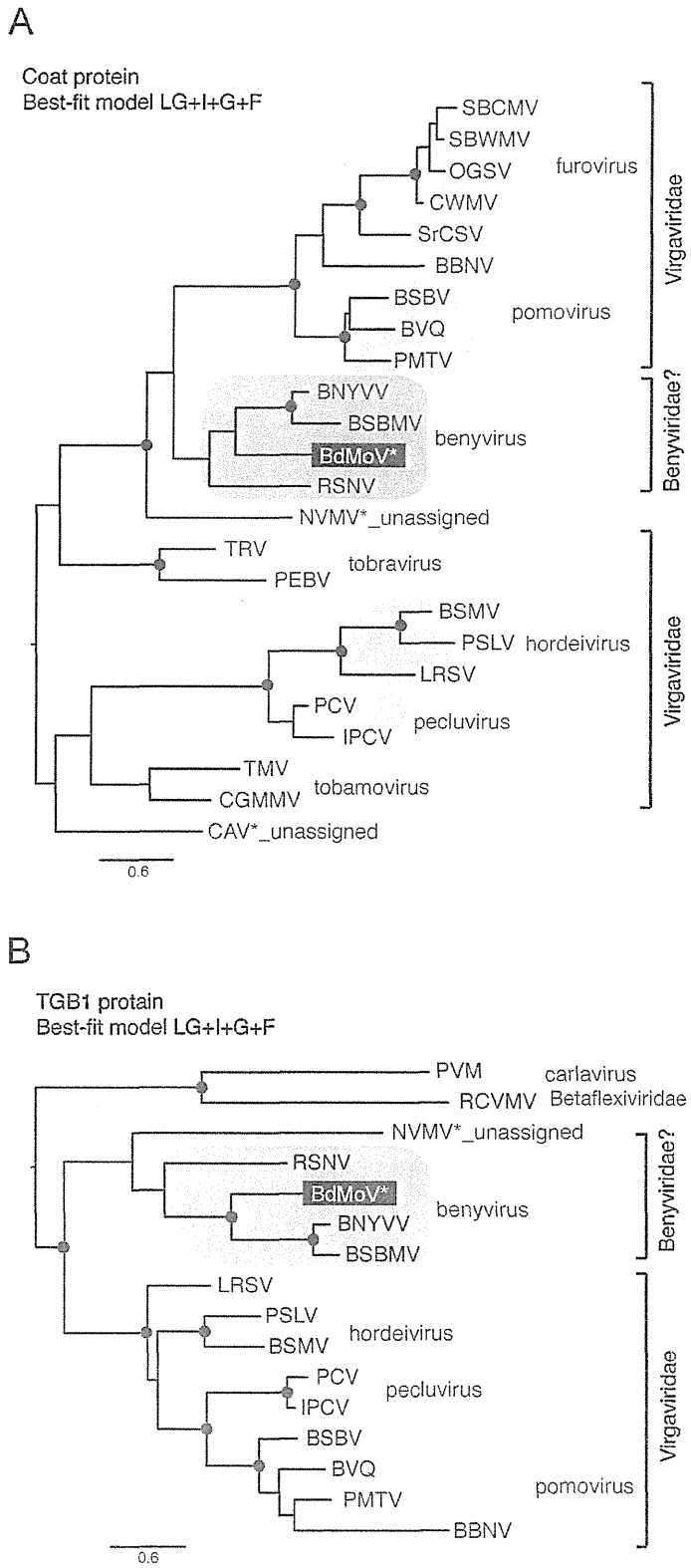


**Fig. 4.** Phylogenetic (ML) trees calculated from the coat proteins (A) and TGB1 proteins (B) of BdMoV and benyviruses together with selected rod-shaped viruses included in the family *Virgaviradae*. The alignments of the amino acid sequences were generated with MAFFT (Supplementary Fig. S3C and D). The trees were constructed by the ML method using PhyML 3.0. The nodes with filled circles are supported by aLRT values of greater than 0.9. The scale bars represent the amino acid distances. Carlaviruses (potato virus M [PVM]: AAP76201, red clover vein mosaic virus [RCVMV]: ACN58188) were used as the outgroup for TGB1 analysis. The sequence data of other viruses used for analyses were obtained from the EMBL/DDBJ/Genbank and are listed in Supplementary Table S2.

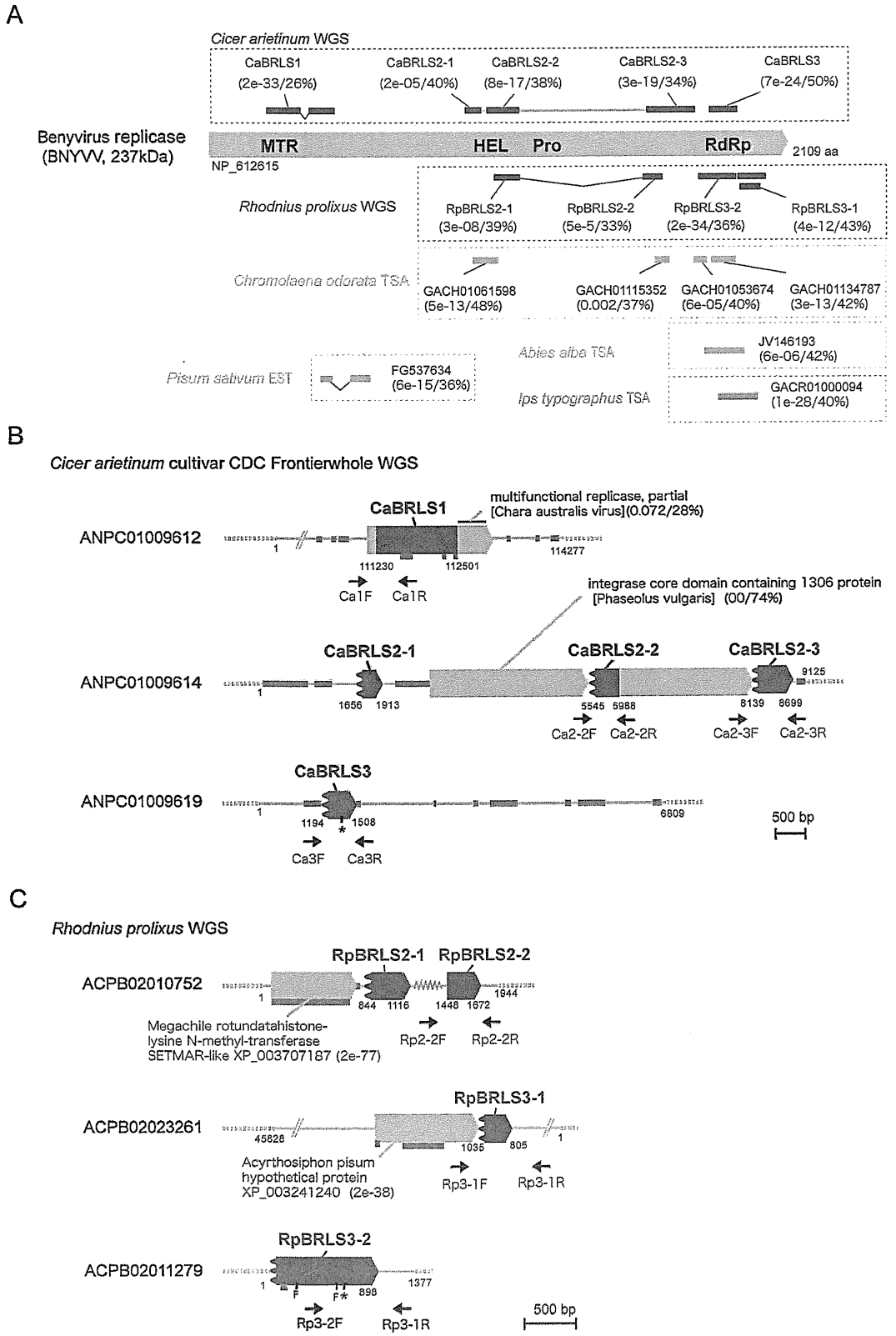


**Fig. 5.** Schematic representation of *Cicer arietinum* (CaBRLS) and *Rhodnius prolixus* (RpBRLS) benyvirus replicase protein-like sequences and their flanking regions. (A) The corresponding positions of BRLSs on the benyvirus replicase. The box shows a diagrammatic representation of the conserved domains of BNYVV replicase protein. (B and C) BRLSs found in the whole-genome shotgun (WGS) database of chickpea plant (*C. arietinum* L) (B) and blood-sucking insect (*R. prolixus*) (C) are shown to match the replicase protein from BNYVV in (A). The potential coding regions of BRLSs and flanking ORFs are shown as boxes. Retrotransposon-like sequences are shown by thick gray lines. The positions of the primers used for genomic PCR (see Fig. 6) are shown by arrows. The WGS-assembled sequences and undetermined sequences are shown by solid and dashed thin-lines, respectively. Symbols referring to potential mutations are also shown: kinked line, major deletion; asterisk, internal stop codon; F, frame-shift.

most likely the transmembrane regions (TM1 and TM2) commonly found in the RT domains or P2 regions of viruses with plasmodiophorid vectors. A KTER motif in the TM2 of BNYVV and BSBMV, which is important for efficient transmission (Tamada et al., 1996), was not detected in the TM2 of BdMoV and RSNV. The C-terminal regions of the RT proteins consist of relatively large numbers of serine residues, 16 out of the terminal 66 aa (BdMoV), 19 out of 83 aa (BNYVV), 21 out of 105 aa (BSBMV) and 22 out of 100 aa (RSNV).

The central region of BdMoV RNA2 contains the TGB-like structure that is possibly required for benyvirus cell-to-cell movement (Lauber et al., 1998) (Fig. 2). A similar TGB-like structure is found in NVMV (Randles and Rohde, 1990). The first TGB protein (TGB1) contains the conserved dNTP binding-site motif GxxGxGKS (x = any aa), in positions 92–99 (Richards and Tamada, 1992; Solovyev et al., 2012) (Supplementary Fig. S2B, TGB1). BNYVV and to a lesser extent BSBMV TGB1 have a K/R-rich cluster on the N-terminal 30 residues, whereas this region is absent in the BdMoV and RSNV TGB1. Hydrophobicity plot analysis for BdMoV TGB2 and TGB3 proteins shows that both proteins have two hydrophobic regions (data not shown). These regions are predicted as potential transmembrane domains using the TMHMM Server v.2.0 (www.cbs.dtu.dk/services/TMHMM), supporting the hypothesis that the TGB2 and TGB3 proteins bind to membranes (Supplementary Fig. S2B, TGB2 and TGB3). BdMoV TGB2 contains a semi-conserved sequence, $GDx_6GGxYxDG$, in the central region, whereas TGB3 does not have the proposed motifs, $Ax_7Px_{12}KxxDA$ in the center and WFWxH in the C-terminal regions (Morozov and Solovyev, 2012; Solovyev et al., 2012).

The ML tree of the TGB1 aa sequences showed that BdMoV is clustered with benyviruses, which is distantly related to the pecul-, hordei- and pomoviruses, but less distantly related to NVMV (Fig. 4B). The BdMoV TGB1 protein is 42 to 48% identical to those of other benyviruses and 32% identical to NVMV TGB1 (Table 1). Similar trends were observed in the ML trees of TGB2 and TGB3 (data not shown).

Database searches for BdMoV CRP did not reveal substantial identity with any known protein (Table 1). When aligned with other benyvirus CRPs, four conserved cysteine residues (aa positions 55, 58, 92 and 95) were identified in their central regions, as described previously (Chiba et al., 2013) (Supplementary Fig. S2B, CRP). The CRPs of BdMoV, BNYVV and BSBMV have been shown to function as the weak transgene silencing suppressors in leaf tissue (Andika et al., 2012; Chiba et al., 2013; Guilley et al., 2009). BdMoV p13 CRP accumulated in the nucleus (data not shown), whereas BNYVV p14 and BSBMV 14-kDa CRPs were distributed in the nucleolus and cytoplasm in which nucleolar localization is not required for its silencing-suppression activity (Chiba et al., 2013).

### 3.5. *The discovery of benyvirus replicase-like sequences (BRLS) in plant and insect genomes.*

We searched for the presence of benyvirus-related sequences in the eukaryotic genomes that are available in NCBI databases. Using benyvirus sequences as queries, we found six significant matches to BdMoV replicase aa sequences in the whole-genome shotgun (WGS) assemblies of the chromosomes of the chickpea plant (*Cicer arietinum* L., cultivar = CDC Frontier, family *Fabaceae*) and the blood-sucking bug (*Rhodnius prolixus*, family *Triatomidae*) (Fig. 5A). Based on the nomenclature system for integrated non-retrovirus RNA viral sequences (Chiba et al., 2011b), these novel sequences were termed *Cicer arietinum* benyvirus replicase protein-like sequences 1–3 (CaBRLS1–3) and *Rhodnius prolixus* BRLSs 2–3 (RpBRLS2–3) (Fig. 5B and 5C). Reverse BLAST analysis using their potentially encoded proteins revealed 26–50% aa identities ($E$-value = $2e^{-5}$–$2e^{-33}$) for CaBRLSs and 33–39% aa identities ($E$-value = $5e^{-5}$–$8e^{-43}$) for RpBRLSs in the corresponding region in the BNYVV replicase protein (237 kDa) (Fig. 5A).

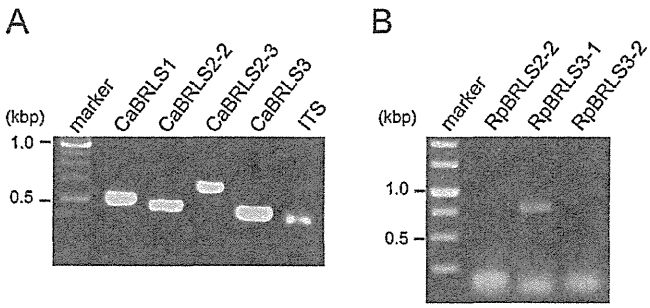


**Fig. 6.** Genomic PCR analysis of BRLSs. CaBRLSs of the chickpea plant (A) and blood-sucking insect samples (B) were amplified using a primer set specific for each BRLS (Fig. 5B and C). Two primer sets, At-IRS-FW and At-IRS-RV (Chiba et al., 2011b), and 5.8T Rp-ITS2F and 28T Rp-ITS2R (Marcilla et al., 2001) were used for amplification of the plant and insect (data not shown) ITS regions, respectively.

In addition, we also found that another WGS library onto the *C. arietinum* chromosome (cultivar ICC4958), which was very recently released from the NCBI site, contains mostly identical sequences to each CaBRLS from the chickpea cultivar CDC Frontier. All BRLSs have distinguishable flanking sequences of the host origin in which CaBRLS2 and RpBRLS2 contain trace putative plant (DNA/Mariner class) and insect (LTR/Copia class) transposable elements, respectively (Fig. 5B and C).

To confirm the presence of BRLSs in the chickpea plant and the blood-sucking insect chromosomes, genomic PCR detection was performed. To this end, different sets of primers for each of the CaBRLSs and RpBRLSs were designed (Fig. 5B and C, indicated by arrows). As expected, PCR products of the expected sizes were obtained for all primer sets on genomic DNA from the chickpea plant (Fig. 6A). For RpBRLSs, a DNA fragment was only amplified by PCR using the RpBRLS3-1 primer set specific for the blood-sucking bug genomic DNA, but not using RpBRLS2-2 and 3-2 primer sets (Fig. 6B). The same results were obtained by using additional sets of RpBRLS2-2 or 3-2 primers (data not shown). The sequences of PCR fragments derived from the chickpea and blood-sucking bug samples were identical to the corresponding regions of the CaBRLSs and RpBRLS3-1 sequences from databases (data not shown). These results suggested that the CaBRLSs are probably widely present in chickpea cultivars, whereas RpBRLSs and/or their harboring *R. prolixus* chromosomes are more divergent in the strain or isolate level.

In order to evaluate the relationships of BRLSs and related viruses, we conducted ML analysis based on aa alignment of each of three replicase domains (MTR, HEL and RdRp) of the viruses. This analysis included replicase sequences of benyvirus-related viruses, such as animal hepeviruses, insect tetraviruses, animal rubiviruses, a mycovirus (SsRV-L) and an alga virus (CAV). As shown in Fig. 7, it is clear that CaBRLSs and RpBRLS are closely related to the clade of benyviruses. Notably, the BRLSs show a closer relationship to the replicase of CAV than to those of other animal, insect and fungal viruses, and this provides details of the genealogy of this unique alga virus and benyviruses (Fig. 7).

Several studies have demonstrated that the transcriptome analysis based on next-generation sequencing technologies is a useful new research tool for the discovery of RNA viruses (Kristensen et al., 2010; Radford et al., 2012). During BLAST searching for BRLSs using the benyvirus replicase aa sequences as queries (e.g., BNYVV), interestingly, we found several significant matches in the transcriptome shotgun assembly (TSA) library databases (Fig. 5A), i.e., four matches (GeneBank accessions GACH01061598, GACH01134787,